國立臺灣大學生命科學院漁業科學研究所

碩士論文

Institute of Fisheries Science

College of Life Science

National Taiwan University

Master Thesis

北南海浮游植物生物量(葉綠素-*a*)之多時間尺度變化分析

Multi-scale temporal variation in phytoplankton biomass

(chlorophyll-*a*) in the northern South China Sea

侯力慈

LI-TZU Hou

指導教授: 柯佳吟 博士

Advisor: CHIA-YIN Ko, Ph.D.

民國 108 年 7 月

July 2019

謝辭

計畫總是趕不上變化,念碩士班的兩年中也出現很多驚喜,帶著兩個兒子念書,雖然過程跌跌撞撞,好幾度想要放棄,終於還是完成了這篇論文。首先要感謝指導教授柯佳吟老師給予我這個學習的機會,以及一路上的督促、包容與用心指導,帶領我從一開始毫無頭緒的研究到完成這篇論文。感謝夏復國老師無私的指導、提供珍貴的南海資料、指引我研究的方向與論文寫作上的指導。也要感謝陳宗岳老師與王博賢老師在海洋科學知識與論文上的指教,以及他們的支持與鼓勵。

此外,也要感謝實驗室的夥伴們的陪伴與照顧,穎禎、旻祐、馬霽、晴芳、思維、幸慈、成姊與光瑢姊、漁科所的老師與同學們,以及中研院的老同事們。雖然大家的研究領域不盡相同,但大家還是很認真的聽我的報告、給予我研究上的意見,也總是很熱情的當小保姆們陪我的兩個小皮蛋兒子、在生活上給予我協助。在實驗室的時光總是很歡樂,讓我在研究的路上不孤單。

這篇論文集結的過去二十幾年來 30 個航次的資料,這些數據的背後是幾十位研究員、老師、研究助理、學生、船員、探測員等等的汗水、淚水、暈船與熬夜的付出。所以,也要感謝這些第一線偉大的海洋研究者對臺灣海洋科學的貢獻與付出。最後,也要感謝我的家人,我的兩個爸爸媽媽、大姊、姊夫、小妹、小姑、小 Zac、小 Mason,還有我最愛的老公文軒,這段期間有大家的包容與支持才得以完成這篇論文。
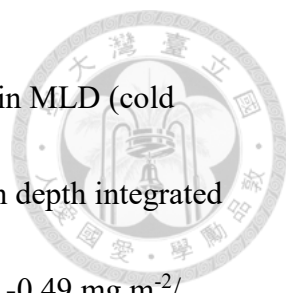
中文摘要

　　浮游植物是海洋生態系統的主要生產者,並在食物鏈中扮演重要的角色。它的豐度和分布與水溫、營養鹽、光和浮游動物的掠食有關,且亦受季節、天氣和混合層深度(Mixed layer depth,簡稱 MLD)影響。本研究整理南海北部的南海時間序列測站(SEATS,116°E 和 18°N)在 1999-2019 年間收集到的 30 次航次資料,進行水層中葉綠素-*a*(Chlorophyll-*a*,簡稱 Chl-*a*)濃度的"日變化"、"季節變化"及"超過十年變化"的多時間尺度分析。結果顯示在"日變化"中,Chl-*a* 濃度在白天逐漸增加至傍晚時最高,隨後減少至黎明前最低,在冬季時,最大值與最小值差可達 2 倍;Chl-*a* 濃度與混合層深度(Mixed layer depth,簡稱 MLD)或海表溫度在"日變化"中沒有顯著相關性。在"季節變化"分析中,冬季(十二月和一月)的 MLD 較深使得 Chl-*a* 濃度均勻分布於表層且高於其他月份;此外,航次間的表層 Chl-*a* 濃度與有光層積分 Chl-*a* 濃度值分別與海表溫度和 MLD 有顯著相關。在"超過十年變化"的長時間尺度上,隨著海表溫度的上升(冬季: $0.05\,°C$/年; 其他月份: $0.06\,°C$/年),混合層深度亦隨之變淺(冬季: $-0.80\,m$/年; 其他月份: $-0.52\,m$/年),這使得 SEATS 測站浮游植物生長所需的底層營養鹽輸入程度變小,最終造成有光層積分 Chl-*a* 濃度下降(冬季: $-0.73\,mg\,m^{-2}$/年; 其他月份: $-0.49\,mg\,m^{-2}$/年)。結果表示,由於採樣的時間點可能造成 Chl-*a* 濃度的差異,在進行浮游植物濃度變化及初級生產力研究時,需考量短時間的日夜波動。而在二十年變化的分析中,本研究發現隨著海平面水溫升高及混合層深度變淺,表水 10 米水深的 Chl-*a* 濃度及 100 米有光層 Chl-*a* 濃度積分值逐年降低,可能造成南海北部生態與資源的變動。

關鍵詞: 浮游植物、葉綠素-*a*、表水水溫、混合層深度、南海時間序列測站(SEATS)

Abstract

Phytoplankton are major primary producers in marine ecosystems and can directly impact higher trophic levels. The abundance and distribution of phytoplankton are known to be related to water temperature, nutrient, light, and zooplankton grazing. Therefore, the phytoplankton dynamic is often linked to seasonal variations and mixed-layer depth (MLD). This study compiled and analyzed *in situ* fluorescence and chlorophyll-*a* (Chl-*a*) concentration data at the SouthEast Asia Time-series Study (SEATS, 116°E and 18°N) station in the northern South China Sea, to understand the phytoplankton dynamics in different time scales, diurnal, seasonal, and decadal scales. *In situ* Chl-*a* concentrations and water temperature were collected for 30 cruises throughout 1999 and 2019 at the SEATS station, and the euphotic depth integrated Chl-*a* concentrations were analyzed and compared with sea surface temperature (SST) and MLD. In the diurnal scale, the results showed the Chl-*a* concentrations increased during the day, decreased during the night time, and the variations could be as high as two-fold. In the seasonal scale, the Chl-*a* concentrations, SST and MLD showed two distinct patterns: the cold seasons (December and January) with low SST, deep MLD, and high Chl-*a* concentrations; the warm seasons (March to November) with high SST, shallow MLD, and low Chl-*a* concentrations. Seasonal Chl-*a* concentrations, SST and MLD also showed correlations. In the decadal scale, the 20-year data showed an increase in SST

(cold season: 0.05 °C/ year; warm season: 0.06 °C/ year), a decrease in MLD (cold

season: -0.80 m/ year; warm season: -0.52 m/ year), and a decrease in depth integrated

Chl-*a* concentrations (cold season: -0.73 mg m^{-2}/ year; warm season: -0.49 mg m^{-2}/

year) at the SEATS station. The results suggest that, in short-term study, it is important

to consider the diel fluctuations when conducting field sampling for phytoplankton and

primary productivity studies; in the 20-year analysis, the increase of SST and the

shallowing of MLD led to the decrease in Chl-*a* concentrations, and which may impact

the ecology and resources in the northern South China Sea.

Keywords: phytoplankton, chlorophyll-*a*, sea surface temperature, mixed layer depth,

the SouthEast Asia Time Series (SEATS) Station

Table of Contents

List of Figures

List of Tables

Chapter 1. Introduction

1.1 Primary production and phytoplankton

Primary production is the process where photosynthesis utilize inorganic carbon and transform it to organic carbon molecules, with the presence of sunlight, water, air and nutrients. Marine primary production is mainly conducted by phytoplankton, which is photosynthetic microscopic drifting plankton, and this tiny marine phytoplankton accounts for approximately half of the global primary production, which is about 50 petagrams of carbon per year (Field et al., 1998). As primary producers, the abundance and distribution of phytoplankton can further impact higher trophic levels, fishery, then the whole ecosystem (Boyce et al, 2010). Therefore, understanding phytoplankton dynamic is critical for future estimation of marine ecosystem changes and resources.

Phytoplankton occurs in the euphotic zone (< 200 m) where light can penetrate through to offer sufficient energy for photosynthesis. The euphotic zone depth is usually defined as the depth where 1% of its surface photosynthetic available radiation (PAR) value (Ryther, 1956). The euphotic zone can be as deep as 200m, but also can be as shallow as a few meters in turbid coastal eutrophic water. Below the euphotic zone, phytoplankton detritus sinks and remineralize into inorganic nutrients such as nitrate and phosphate, which are enriched in the deeper water. Nitrogen (nitrate, nitrite or

ammonium) and phosphorous (dissolved inorganic phosphorous) are the two major

essential nutrients for phytoplankton growth. Silicate is also another major nutrient for

species such as diatoms that required silicon for their shells. Other trace metals, such as

iron, copper, and zinc are also essential for phytoplankton growth (Falkowski & Raven,

2013; Morel & Price, 2003).

Water column stratification is an important factor controlling nutrient supply to

phytoplankton in the surface water. The vertical gradients of temperature and density

separates the ocean water column into layers. When the gradient of temperature and

density is large the water column is more stratified; when the gradient is small, less

stratified water allows the deep and surface water to mix vertically. Other physical

forcing, such as wind and upwelling, can also create vertical mixing that bring the

nutrient rich deep water up to the surface. The spatial distribution and abundance of

phytoplankton reflects the light and nutrient supply conditions in the water column. In

coastal areas, river runoffs and upwelling bring high nutrients and productions, which

can be two orders of magnitude higher than oligotrophic open ocean surface water

(Chavez et al, 2011; Sarmiento & Gruber, 2006). In open ocean, phytoplankton depends

on the bottom up input of nutrient to the euphotic zone (eg. eddies, winter winds). At

high latitudes, seasonal mixing dominates the nutrient supply, but in tropical margins,

nutrient supply to the euphotic zone is mainly due to climate-driven fluctuations in the

depth of the thermocline (Letelier et al., 1993). In the open ocean sub-tropical gyres, the

nutrients are supplied by turbulent mixing along the thermocline and this process can be

amplified by mesoscale eddies and supplemented by nitrogen fixation (Chavez et al.,

2011). Phytoplankton dynamics could be regulated by a combination effect of weather

and oceanographic processes and it varies spatially and temporally. Marine biologists

are in search of the links between these physical processes and biological response, not

only to use physical oceanographic parameters as indicators for phytoplankton dynamic,

but also to predict phytoplankton dynamics under future environmental changes.

1.2 Hydrographic factors on phytoplankton dynamic

1.2.1 Sea Surface Temperature

Temperature can have direct effect in the metabolism and growth of phytoplankton

(Toseland et al., 2013), but the more significant influence of temperature on

phytoplankton dynamic is the result of water stratification and seasonal fluctuations

(Winder & Sommer, 2012). Sea surface temperature (SST) can directly reflects seasonal

variability of a area and indicates the extent of water stratification. A statistical

reconstruction of Chl-*a* from 1958 to 2008 in the tropical Pacific also correlated with

SST, sea surface height (SSH), and Chl-*a* variance in El Niño-Southern Oscillation

(ENSO) events, and the study showed varied patterns depending on stratification or

3

shoaling of thermocline (Schollaert Uz et al., 2017). Boyce et al. (2010) also compiled

the global phytoplankton concentration and suggested decadal scale fluctuations linked

to climate forcing, and long term declining trends are related to increasing sea surface

temperature.

1.2.2 Mixed layer depth

Many studies have also linked mixed layer depth (MLD) and thermocline with

phytoplankton dynamic (Carvalho et al., 2017; Karl & Church, 2014). Ocean surface

mixed layer is the upper portion of the surface water where an active turbulence has

caused the water to mix vertically and homogenized in temperature and salinity. The air-

sea exchange turbulence could be generated by winds, surface heat fluxes, and

processes such as evaporation or sea ice formation which result in an increase in

salinity. The mixed layer determines the average level of light utilized by marine

organism, and it defines a critical depth where irradiation and temperature are suitable

for phytoplankton growth and intrusion of nutrient rich water below the mixed layer

(Cronin & Sprintall, 2009; Gardner et al., 1995; Kara et al., 2000). *In situ* measurement

carried out by Carvalho et al. (2017) showed a 1:1 relationship between MLD and Chl-*a*

maxima depth in Antarctica coastal seas, and they proposed the possibility to use MLD

as an indicator for biologically activities. Because mixed layer varies with temperature

4

and wind, the MLD may be altered by extreme weather events or global temperature

increase, then the phytoplankton growth may be further impacted, so as for biomass and

community structure in the upper water column.
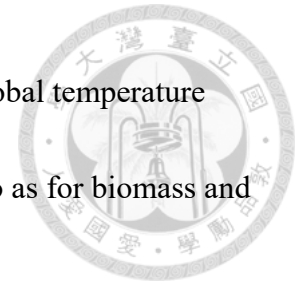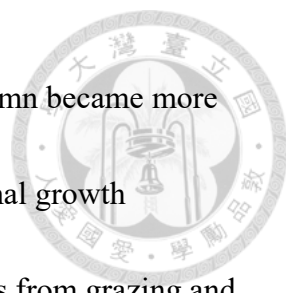
1.3 Temporal phytoplankton dynamic

1.3.1 Diurnal variations

The diurnal variation of phytoplankton has been shown in various locations and

studies and it is highly related to physical, biological or physiological processes

(Neveux, 2003; Wood & Corcoran, 1966; Woods & Onken, 1982). Studies in the

equatorial Pacific showed that Chl-*a* diurnal variation was related to the balance

between growth and mortality of phytoplankton, cellular physiological responses to

environmental modifications such as photoacclimation, and the effects of external

physical factors such as vertical mixing, internal waves, advection and sinking (Claustre

et al., 1999; Neveux, 2003; Vaulot & Marie, 1999).

1.3.2 Seasonal variations

At high latitudes, phytoplankton generally shows a distinct seasonal pattern of

bloom in spring. In winter, strong wind-driven turbulence disturbed the water column,

and brings up nutrients from deep water up to the surface euphotic zone. In spring, wind

5

weakens, temperature and light availability increases, and water column became more

stratified with the warning of the surface water. This creates an optimal growth

condition of high nutrients, high light availability, and minimal losses from grazing and

vertical mixing for phytoplankton to grow rapidly (Falkowski & Raven, 2013; Winder

& Cloern, 2010). In spring bloom, phytoplankton can double at least once per day,

allowing for exponential increases in stock size. Later in summer, phytoplankton

abundance decreases due to nutrient depletion in the stratified water column and grazing

from zooplankton. Then again in winter, strong wind and cooling break down the

stratified water column and allows vertical mixing replenishes nutrients from deep

water to the euphotic zone. In these regions, the winter mixing depth dictates the

nutrients available for spring, and the mixing depth varies years to years by wind speed

and stratifications (Chavez et al., 2011, Winder & Cloern, 2010). At lower latitude, long

term phytoplankton study in Hawaii at Station ALOHA (HOTS) between 1989 and

1991 documented variability in phytoplankton abundance and composition, and the

seasonal patterns in Chl-*a* were also found to be depth-dependent, where in the winter,

mixed layer deepens and lead to increase in Chl-*a* in the mixed layer by

photoadaptation; in spring, increases in Chl-*a* is due to increase nutrient availability

caused by a deepening of the deep chlorophyll maximum layer (Karl & Church, 2014;

Letelier et al., 1993). At lower latitudes, seasonal patterns are less significant, where

6

thermocline shoaling and upwelling is the main supply processes for phytoplankton concentration dynamic. The wind-driven surface flow with the earth's rotation causes the thermocline to shoal or upwell, particularly at the margins of the subtropical gyres, and nutrients are lifted into the euphotic zone with an increase phytoplankton growth (Chavez et al., 2011).

1.3.3 Interannual to Decadal variations

Interannual to decadal variation of Chl-*a* may be due to the effects of leading climate oscillators, such as ENSO or the North Atlantic Oscillation, and long-term trends in phytoplankton could be linked to changes in vertical stratification and upwelling, aerosol deposition, ice, wind and cloud formation coastal runoff, ocean circulation or trophic effects (Boyce et al., 2010). Previous studies have proposed different predictions in phytoplankton dynamics. Boyce et al., (2010) reconstructed and analyzed the global satellite derived phytoplankton concentration and showed a global phytoplankton decline since 1899 with strong correlation between SST and Chl-*a*. They also suggested that the effects of SST on Chl-*a* can be attributed to its influence on water column stability and MLD. When temperature increases, mixed layer became shallower and limits nutrient supply in stratified tropical waters, but the increase of temperature could also benefit phytoplankton at higher latitudes where growth is

7

constrained by light availability and deep mixing (Boyce et al., 2010). On the other

hand, Chavez et al. (2011) compiled 21 time-series data and concluded an increase in

global Chl-*a* and primary production over the recent 20 years, and showed the

variability of Chl-*a* in some area can be associated with SST (Chavez et al., 2011).

Climate events can alter phytoplankton growth, but the process is complicated, and

many variability and anomalies are still unresolved. Overall, temperature and MLD

changes are still the two important factors in causing long term variations of Chl-*a*,

therefore, this study was to evaluate the changes of Chl-*a* in a long term time series

station in the northern South China Sea in relation to SST and MLD.
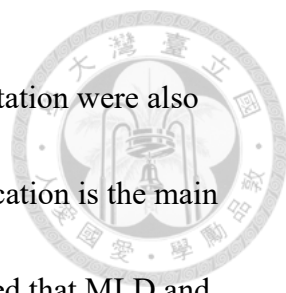
1.4 The SouthEast Asian Time-series Study (SEATS) station

The South China Sea (SCS) is one of the largest marginal seas in the world with

high marine primary production and fish production (Qiu et al., 2010). Located in the

tropical zone, the SCS stretches from about 22°N at the southern coast of the Taiwan

Island and the Chinese Mainland to 4°N at the coasts of Borneo and Sumatra, and from

105°E along the east coast of the Malay Peninsula to 121°E along the western coasts of

the Philippine Islands. In the northern SCS, there is strong northeast monsoon winds

between November and April, and weaker southwest monsoon between June and

September; about two-thirds of the precipitation occurs between June and September

8

when the southwest monsoon brings warm humid air, and evaporation exceeds

precipitation from October to April when the northeast monsoon brings cold dry air to

the area (Wong et al., 2015). The major current in the SCS changes direction responding

to the monsoons, where the northeast monsoon in winter drives a cyclonic gyre, and the

southwest monsoon in summer causes reversal of the gyre in the southern part of the

basin (Shaw & Chao, 1994). Previous studies observed the MLD in the northern SCS is

about 40 m in the summer and 70m in the winter, which is relatively shallow to the

global MLD, and the MLD at the SEATS station has been reported to be about 20m

deep in the summer and 70 m in the winter (Tai et al., 2017; Wong, Ku, et al., 2015).

Chl-*a* obtained from satellite data showed two chlorophyll maxima in December-

January and July during the heights of the monsoonal season at the SEATS station

(Wong, Pan, et al., 2015), and it has relatively distinct seasonal pattern than other

tropical latitude waters (Tseng, 2005).

A previous study at SEATS station showed that remote sensing datasets of surface

Chl-a correlates to SST, SSH, wind and ENSO from 1997 to 2012, and the correlations

between Chl-a and SST to wind speed are stronger during El Nino years, which could

be due to the deepened thermocline when wind driven nutrient pumping is less efficient

(Liu et al., 2013). Also, a recent study using MODIS satellite analysis also showed a

negative correlation between Chl-a and SST (Liu et al., 2015). Tai et al. (2017) observed

9

the monthly average SST and monthly average MLD at the SEATS station were also

negatively correlated, and that temperature and wind induced stratification is the main

result for MLD variations at the SEATS station. Hence, I hypothesized that MLD and

Chl-a can be positively correlated at the SEATS station. Furthermore, the majority of

these studies used remote sensing data that only consider the surface Chl-*a*, which could

not represent the phytoplankton in deeper water. At the SEATS station, euphotic zone

can be as deep as 100 m in the winter, and the chlorophyll maxima layer is about 50 m

(Liu et al., 2002). The integrated Chl-*a* derived from *in situ* measurement in the

euphotic zone is a much more representative parameter/proxy to reflect phytoplankton

variations in the whole water column. Therefore, I would like to evaluate the *in situ*

euphotic depth integrated Chl-*a* variations for phytoplankton dynamic at the SEATS

station.

1.5 Objectives

Phytoplankton are the ultimate source of organic materials which drive food-web

processes (i.e. grazing food-chain, detritus food-chain, and microbial-loop) and

ecosystem properties (i.e. autotrophic vs. heterotrophic). Phytoplankton biomass is

commonly inferred form measured of total Chl-*a* pigment concentration, and Chl-*a*

could explain the variance in marine primary production and capture the first order

10

changes in phytoplankton biomass (Boyce et al., 2010; Falkowski & Raven, 2013). The

aim of this study was to uncover the signals of phytoplankton biomass at various

temporal scales from the SEATS station locating at the tropical northern SCS by Chl-*a*,

and the driving mechanisms for the algal biomass signals at various scales were also

explored.

Chapter 2. Materials and Methods

2.1 Study location

All of the datasets used in this study were collected at the Southeast Asian Time-

Series Study (SEATS) station, which is located at 18°N, 116°E in the northern South

China Sea (SCS).

2.2 Data

From 1999 to 2019, 38 cruises were conducted at the SEATS station, and 30

cruises with complete Chl-*a* and fluorometer data were selected (Appendix Table A1).

In the selected cruises, anchored samplings were carried out in the 10 cruises from 2010

to 2019. Water column sampling was conducted every 3 hours for more than 16 hours to

monitor the diurnal variations of physical, chemical and biological (Chl-*a*) factors. All

the datasets used in this study are available in the Ocean Data Bank of the Ministry of

Science and Technology, Taiwan (http://www.odb.ntu.edu.tw), maintained by the

Institute of Oceanography, National Taiwan University.

2.3 Measurement of hydrographic parameters

All the hydrographic parameters, including temperature, salinity, conductivity,

density, oxygen, transmission, and PAR were recorded by a SeaBird model SBE9/11

(Sea-Bird Electronics, Inc.) conductivity-temperature-depth (CTD) profiling recorder

during every deployment. SST is the main temperature representation used in this study,

and for the consistency between cruises, the sea water temperature at 10m depth were

used to represent SST in this study.

2.4 Chl-*a* fluorescence

For phytoplankton biomass, chlorophyll fluorescence was measured by a

fluorometer (Fluorometer Aqua Track III) equipped on the CTD. During each research

cruise, discrete sea water samples were collected by Go-Flo bottles mounted on a CTD

rosette at the selected water depths (eg. 5m, 10m, 20m, 50m, 80m and 100m) for Chl-*a*

analysis. Two liters of sea water were collected by a 2L dark polypropylene bottles and

filtered on board through 47mm GF/F filters (Whatman) under vacuum pressure less

12

than 100 mmHg. After filtration, the filters were then preserved in tissue embedding

cassettes and were frozen in liquid nitrogen and kept under -20°C until further

processing in a shore-based laboratory. The samples were extracted by 90% acetone and

measured either by HPLC (Shimazu LC-10A, method refers to Ho et al., 2015) or

fluorometer (Turner 10-AU, method refers to Strickland and Parsons, 1968), with Chl-*a*

standard validated by an UV-vis spectrophotometer and fluorometer for calibration.

HPLC, fluorometric, and the traditional spectrophotometric methods were known to

have good agreements in measuring marine Chl-*a*, and the results from all methods are

comparable (Murray et al., 1986). Fluorescence measured by a fluorometer, f, can be

expressed as : $f = Ea^* \Phi$ Chl-*a*, where E is the intensity of the excitation source (mole

quanta m^{-2} s^{-1}), a^* is the specific absorption coefficient (m^2 mg Chl-*a* $^{-1}$), Chl-*a* is the

chlorophyll-a concentration (mg Chl-a m^{-3}) and Φ is the fluorescence quantum yield

(mole quanta emitted mole quanta absorbed $^{-1}$) (Mignot et al., 2011). The calibration of

the fluorescence measurements against true Chl-*a* measurement is acquired to

eliminate the variations of the instrument, such as light source intensities and detector

as much as possible. For each cruise, the CTD fluorescence were verified and calibrated

with the discrete Chl-*a* measurements by linear regressions (Appendix Table A3). This

calibrated chlorophyll fluorescence (F$_{Chl-a}$) were used to present Chl-*a* in this study.

Due to the complexity of phytoplankton photosynthesis process, phytoplankton

13

biodiversity, and the difficulty to obtain large amount of *in situ* measured phytoplankton

biomass, I here present the calibrated fluorescence data to observe the phytoplankton

dynamic with awareness that the fluorescence is not a direct representation of

phytoplankton biomass. Definition for the abbreviations mentioned in this study were

shown in Table 1.

2.5 Euphotic depth integrated Chl-*a* and surface Chl-*a*

The euphotic depth integrated Chl-*a* concentrations [F_{Chl-a}] in the water column

were calculated by the trapezoidal integration method of the F_{Chl-a} from 5 meters depth

to 100 meters depth. For the surface Chl-*a*, to be consistent between cruises, the F_{Chl-a} at

10m depth ($F_{Chl-a-10m}$) were selected to represent surface Chl-*a* concentrations.

2.6 Mixed layer depth

In this study, the mixed layer depth (MLD) is defined by a fixed temperature

difference schemes, which is the depth with temperature that is 0.8°C lower than the

reference temperature at 10m (Tai et al., 2017).

2.7 Data analysis

Temperature and chlorophyll contours were drawn by software Ocean Data View.

14

Figures and simple statistical analysis were presented and carried out by Sigmaplot. Pearson's correlation analysis was applied between each parameter of $F_{Chl-a-10m}$, $[F_{Chl-a}]$, SST and MLD, and with significant level of $\alpha=0.05$. ANOVA and Mann-Whitney Rank Sum Test were applied to test significant differences between samples and groups with significant level of $\alpha=0.05$. Coefficient of variation (CV= mean/ standard deviation x 100%) was applied to compare variations between samples.
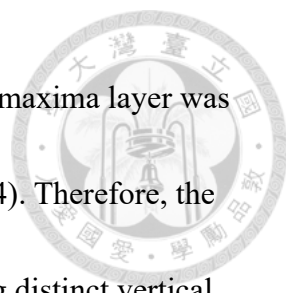
Chapter 3. Results

3.1 Temperature and Chl-*a* profile

From 1999 to 2019, 30 cruises at the SEATS station showed an average of 23.51 mg m^{-2} for $[F_{Chl-a}]$, with the lowest at 12.03 mg m^{-2} in March 2002 (OR1-639), and highest at 45.48 mg m^{-2} in November 2002 (OR1-664) (Table 2). For $F_{Chl-a-10m}$, the average of 30 cruises was 0.17 mg m^{-3}, with the lowest concentration of 0.04 mg m^{-3} in Nov 2017 cruise (OR1-1184), and the highest concentration was in December 2003 cruise (OR1-705) of 0.60 mg m^{-3} (Figure 2 and Table 2). The average SST at 10m of the 30 cruises was 26.75 ± 2.07 °C, and the average MLD was 52.79 ± 23.33 m.

In December and January, the Chl-*a* depth profile shows a uniform profile with relatively even distribution of high Chl-*a* at the upper 50 m water column, while for

15

other months, the surface Chl-*a* was low and subsurface chlorophyll maxima layer was presented between 50 m depth and 80 m depth (Figure 2 and Figure 4). Therefore, the seasons at the SEATS station were divided into two seasons, by using distinct vertical profiles of fluorescence, temperature, and density (Figure 4). The cruises between March and November (n=21) were classified as the warm season, and the cruises between December and January (n=9) were classified as the cold season. In the cold season, the average SST was 24.36 ± 0.70 °C, the MLD was 80.51 ± 13.00 m, the [$F_{Chl\text{-}a}$] and $F_{Chl\text{-}a\text{-}10m}$ were 29.55 ± 8.07 mg m^{-2} and 0.32 ± 0.14 mg m^{-3} respectively. In the warm season, the average SST was 27.77 ± 1.52 °C, the MLD was 40.90 ± 15.08 m, the [$F_{Chl\text{-}a}$] was 20.92 ± 8.25 mg m^{-2}, and the $F_{Chl\text{-}a\text{-}10m}$ was 0.11 ± 0.01 mg m^{-3}. The SST in cold season was significantly lower than the warm season (Mann-Whitney Test, $p<0.001$); the MLD in the cold season was significantly deeper than the warm season (Mann-Whitney Test, $p<0.001$), and both [$F_{Chl\text{-}a}$] and $F_{Chl\text{-}a\text{-}10m}$ were significantly higher in cold season than warm season (Mann-Whitney Test, $p=0.009$ and $p<0.001$, respectively) (Figure 3). In the cold season, Chl-*a* were evenly distributed above the MLD (Figure 4a). While for the warm season, the $F_{Chl\text{-}a\text{-}10m}$ concentrations were low, but a high Chl-*a* subsurface chlorophyll maxima layer was observed underneath the MLD (Figure 4b).

16

3.2 Diurnal variations

Diurnal time-series measurements were carried out in 10 cruises from 2010 to 2019 (total duration of 24 to 36 hours with CTD deployment and sampling per 3 hours) to investigate the diurnal variation of the $[F_{Chl-a}]$ and $F_{Chl-a-10m}$ at the SEATS station. Figure 5 showed that $[F_{Chl-a}]$ increased during the day time, with the highest concentrations observed in the late afternoon, and $[F_{Chl-a}]$ decreased after 6 pm, and became the lowest around 6 am just before dawn. For the $F_{Chl-a-10m}$, the diurnal variations were much significant in the cold season (solid blue symbols) than the other cruises in warm season (open red symbols) (Figure 6). In the three cold season cruises, $F_{Chl-a-10m}$ also decreased during the night time, but continued to decrease in the morning, with the lowest concentrations around noon time. $F_{Chl-a-10m}$ increased in the afternoon and reached the highest around 6 pm. The $F_{Chl-a-10m}$ diurnal variations were less significant in the warm season that the cold season (Figure 6), and no significant pattern was observed for the diurnal $F_{Chl-a-10m}$ variations in the warm season (Figure 7). The diurnal sampling coefficient of variance (CV) of $[F_{Chl-a}]$ ranged from 5% to 24%, and the CV of $F_{Chl-a-10m}$ ranged from 4% to 23% (Table 2).

3.3 Seasonal variations

The statistical monthly averages of SST, MLD, $[F_{Chl-a}]$, and $F_{Chl-a-10m}$ from 30

17

cruises between 1999 and 2019 were calculated to study seasonal variations at the

SEATS station (Table 3). The monthly averaged SST showed the highest value in July

with 29.77 ℃, and the lowest temperature in January with 24.07 ℃ at the SEATS

station (Figure 8 and Table 3). The shallowest and the deepest MLD was observed in

May and in January, which were 18.56 and 81.47 m, respectively. The [F_{Chl-a}] was

highest in December with 32.74 mg m^{-2}, and the lowest was in May with 13.17 mg m^{-2}.

For $F_{Chl-a-10m}$, the highest concentration was 0.40 mg m^{-3} in December, and the lowest

concentration was 0.06 mg m^{-3} in May (Figure 8 and Table 3).

3.4 Decadal variations

For decadal variations, the 30 cruises from 1999 to 2019 at the SEATS station, both

cold and warm seasons showed increase in SST (cold season: 0.05 ℃ per year; warm

season: 0.06 ℃ per year) and decrease in MLD (cold season: -0.80 m per year; warm

season: -0.52 m per year) over the past 20 years (Figure 9). [F_{Chl-a}] (cold season: -0.73

mg m^{-2} per year; warm season: -0.49 mg m^{-2} per year) demonstrated decreasing trends

for both cold and warm seasons, but $F_{Chl-a-10m}$ did not show obvious changing trends

(Figure 9).
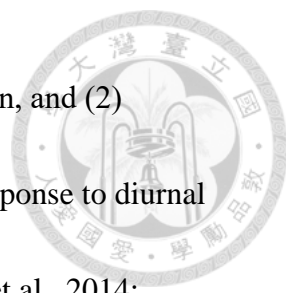
3.5 The relationship between SST, MLD, and Chl-*a*

From monthly average and decadal data, Chl-*a*, SST and MLD tend to show similar patterns. The cruise averaged $F_{Chl-a-10m}$ and $[F_{Chl-a}]$ showed negative correlations with SST (r = -0.61, n = 30, *p* < 0.0001, and r = -0.43, n = 30, *p* = 0.012 respectively) (Figure 10 and 12). While $F_{Chl-a-10m}$ and $[F_{Chl-a}]$ show positive correlation with MLD (r = 0.68, n = 30, *p* < 0.0001, and r = 0.62, n = 30, *p* < 0.0001, respectively) (Figure 11 and 13). There was also a negative correlation between SST and MLD (r = -0.65, n = 30, *p* < 0.0001) (Figure 14), and a positive correlation between $F_{Chl-a-10m}$ and $[F_{Chl-a}]$ (r = 0.73, n = 30, *p* < 0.0001) (Figure 15).

Chapter 4. Discussions:

4.1 Diurnal variations
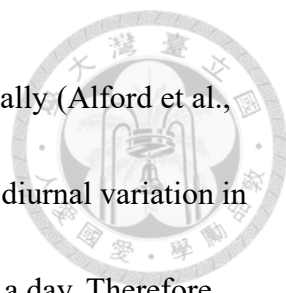
For $[F_{Chl-a}]$ and $F_{Chl-a-10m}$ in the cold season, most of the cruises in this study demonstrated an increase during the day and a decrease at night, which was similar to the general diurnal trend observed in previous studies in the equatorial Pacific (Claustre et al., 1999; Neveux, 2003; Vaulot & Marie, 1999), the North Pacific Ocean (Siegel et al.,1989), and the North Atlantic (Gardner et al., 1995). The Chl-*a* variations were attributed to the combined influences of (1) changes in phytoplankton biomass by

19

growth production and losses due to grazing, sinking, and aggregation, and (2)

phytoplankton photoacclimation and photoinhibition processes in response to diurnal

light availability (Claustre et al., 1999; Letelier et al., 1993; Mignot et al., 2014;

Neveux, 2003). However, carbon (particulate organic carbon, POC) to Chl-*a* ratio was

not evaluated in this study to determine whether the Chl-*a* variations are direct

representation of phytoplankton growth and mortality or photoacclimation process at

the SEATS station.

Apart from the biological processes, Claustre et al. (1999) and Vaulot & Marie

(1999) also showed that the physical vertical mixing could enhance nutrients to the

euphotic zone and the vertical distribution of Chl-*a* in the equatorial Pacific. Our results

at the SEATS station showed some parallel pattern between Chl-*a* and water

temperature isobars in Figure 2, but Pearson's correlation analysis showed no obvious

diurnal correlations between each parameter, including SST, MLD, [F_{Chl-a}], $F_{Chl-a-surf,}$ and

$Z_{Chl-max}$ for each cruise from 2010 to 2019 (Figure A6, Table A2). The variations of SST

and MLD were small in diurnal scale, hence it was difficult to evaluate their influence

on the Chl-*a* variations at the SEATS station. Also, since no completed data were

collected for light intensity, wind, and zooplankton grazing for this study, it was difficult

to identify the exact factors causing the Chl-*a* diurnal variability at the SEATS.

Furthermore, short term events such as typhoons and eddies occur in the northern SCS

20

that could alter the short term phytoplankton and hydrology dramatically (Alford et al., 2015; Zhao et al., 2008). Regardless, the results showed inconsistent diurnal variation in the [F_{Chl-a}] and $F_{Chl-a-10m}$, and the concentrations could double in half a day. Therefore, when investigating short term variability of phytoplankton, it might be important to consider the diurnal effects, and to be aware that a single *in situ* sampling in the field cannot represent the diurnal average. In this cast at the SEATS station, sampling around dawn might under estimate the Chl-*a*, and sampling in the evening might overestimate the Chl-*a*. Overall, diurnally, no significate correlations were observed between SST, MLD, [F_{Chl-a}], $F_{Chl-a-surf}$, and $Z_{Chl-max}$ during the cruises from 2010 to 2019 at the SEATS station.

4.2 Seasonal variations

Similar to previous studies, the Chl-*a* at the SEATS station shows seasonal pattern with highest concentrations in December and January, and lower concentrations during other months. Previous studies suggest that the SEATS station has oceanographic features of shallow nutricline, monsoon-enhanced wind-induced mixing and winter convective overturn by surface cooling, and the semi-enclosed basin that favors a basin-scale upwelling induced by monsoons (Liu et al., 2002, Tseng et al., 2005), and the enhanced vertical mixing by surface cooling and wind-induced mixing in the winter causes the

21
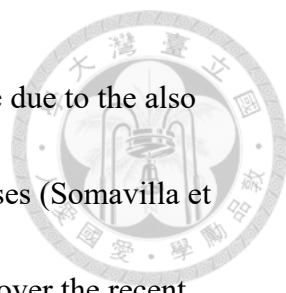
Chl-*a* to increase in winter (Liu et al., 2015; Pan et al., 2015; Tseng, 2005). Since MLD

is the combination result of SST and wind at the SEATS station (Tai et al., 2017), MLD

could indicate the availability of nutrients input to the euphotic zone at the SEATS

station. In December and January, MLD matched with the lower distribution of Chl-*a* in

the surface layer, which indicated that in the cold season, the deep MLD penetrated the

nutricline that bring the nutrient into the upper mixed layer (Cullen, 2015). Hence the

deeper of MLD, the larger the [F_{Chl-a}] will be, and MLD can be used as an indicator for

Chl-*a* vertical distributions in the winter. For the other months (March to November,

warm season) subsurface chlorophyll maxima was observed below the MLD, and

ranged from 10 to 40 m deeper than the MLD. This might be due to the shallow MLD in

the warm season that could not reach the deep nutrient rich water, hence the chlorophyll

maxima depth was located at the depth of the nutricline, and with low Chl-*a* at the

nutrient limited surface water.

The $F_{Chl-a-10m}$ in December was six times higher than May, but the [F_{Chl-a}] in December

was only two times higher than May. When considering the Chl-*a* distribution in the

whole euphotic zone, with the presence of chlorophyll maxima, the seasonal variations

at the SEATS station was less distinctive (Figure 8 c) and d)). The coefficient of

variation (CV) of 30 cruises by months showed large variations that could be up to 50%

for both $F_{Chl-a-10m}$ and [F_{Chl-a}], and the variations were larger than the diurnal CV (Table

3). Short term weather events, interannual ENSO events, and long-term global warming could also impose on this monthly variation, hence resulting higher CVs than diurnal data. However, due to limited cruise sample per year, it was difficult to determine the interannual variations or the influence of medium scale events from our data.

4.3 Decadal variations

Our results show an increase in SST over the 20 years, which could be related to global temperature increase under climate change (Boyce et al., 2010; Pörtner et al., 2014). The warming of the surface water with stratification could reduce the vertical mixing of the upper layer water in northern South China Sea, causing the MLD becoming shallower (Tai et al., 2017). The shallow MLD reduced the nutrient input into the surface ocean, resulting in a decrease in $[F_{Chl-a}]$. Temperature can have direct effect on the phytoplantkton metabolism, but the most significant climatic effects is through changes in thermal stratification patterns such as the extent of the growing seasons and vertical mixing process (Winder & Sommer, 2012). Furthermore, Boyce et al. (2010) suggested that in tropical and subtropical oceans, the effects of SST on Chl-*a* trends are the increasing stratification that limits nutrient supply causing Chl-*a* to decrease, which supports our findings at the SEATS station. In comparison, the MLD did not become shallower with warmer surface water at the North Pacific Subtropical Gyres, the North

23

Atlantic, and the midlatitudes Eastern North Atlantic, which could be due to the also

changing salinity, density, wind-driven divergence and buoyancy losses (Somavilla et

al., 2017), and the integrated Chl-*a* also did not change significantly over the recent

decades at these places (Chavez et al., 2011). At the SEATS station, a decrease in Chl-*a*

in relation to increase SST and shoaling of MLD since 1999 were observed, and with

further increase in global temperature, it is possible that Chl-*a* will continue to decrease

in the northern SCS. Since shallower MLD could be the major cause of the Chl-*a*

variations, the changes in [F_{Chl-a}] could be more significant than $F_{Chl-a-10m}$, and which

could not be observed by remote sensing, and hence highlighting the significance and

importance of field observations.

4.4 The relationship between SST, MLD, and Chl-*a*

Measuring *in situ* primary production and phytoplankton biomass in the deeper

euphotic zone of open ocean could be difficult, hence, using physical processes as

proxies to estimate phytoplankton dynamic could be able to increase our understanding

of the biological process. The results show strong correlations between the [F_{Chl-a}] with

SST and MLD at the SEATS station for each cruise conducted, similar to analysis by

Boyce et al. (2010). Past studies also suggest strong relationship between monsoonal

wind and sea surface heights with phytoplankton dynamic (Liu et al., 2013; Schollaert

24

et al., 2017), hence, combining SST, MLD, and wind forcing data, it is possible to construct a historical or prediction model for the Chl-*a* in the euphotic zone in the northern SCS.

4.5 Further suggestions

Chl-*a* could provide as an indicator for phytoplankton abundance, but it could not fully represent the phytoplankton biomass produced from primary production in a refine scale in some cases. The increase in Chl-*a* in the summer chlorophyll maxima could be due to light induced photoacclimation or by actual increase in phytoplankton production and biomass (Mignot et al., 2014). High zooplankton grazing rate over the rate of primary production will also result in a relatively low Chl-*a* that would under estimate the rate of primary production (Lyngsgaard et al., 2017). Hence, obtaining carbon data for phytoplankton biomass, light intensity, and actual measurement of primary production could enhance our understanding to the phytoplankton and production dynamic at the SEATS station.

Events such as eddies, typhoon and aerosol input could also have influence on the phytoplankton dynamic at the northern SCS, hence combining these weather events and remote sensing data could verify some medium time scale variations in our long-term data trend.

25

Chapter 5. Conclusions

Using the on-board fluormeter with calibration by hand-measured discrete Chl-*a* samples, this study reevaluated the Chl-*a* from the cruises from 1999 to 2019 to construct a more complete and refine temporal phytoplankton dynamic in the whole euphotic zone at the SEATS station. Large diurnal varitions in Chl-*a* were observed that the CV could range from 2 to 42%, and the Chl-*a* could increase two-fold within a day. However, due to the complexity of phytoplankton dynamic and their physiology, it was hard to identify the major cause of the diurnal variation without the support of other parameters. Still, the inconsisdent variations suggest that one time sample could not represent a diurnal average, and more samplings over a diurnal cycle could be a more accurate estimation of the phytoplankton production. For seasonal variability, the SEATS station showed two distintinct seasons, cold season (December and January) and warm season (March to November). Cold season had lower SST, deeper MLD, and higher Chl-*a* than warm seasons. In a decadal scale from 1999 to 2019, an increase trend in SST, decrease in MLD and an decrease in [F_{Chl-a}] were observed, which showed the possibility that shallow MLD causing lower nutirnet input and lower Chl-*a*, and that phytoplankton production could continue to decrease with the current speed of global

26

warming and climate change, and hence reflecting the importance of a long term time

series station in monitoring long term environmental changes.

References

Alford, M. H., Peacock, T., MacKinnon, J. A., Nash, J. D., Buijsman, M. C., Centurioni, L. R., Chao, S-Y., Chang, M-H., Farmer, D. M., & Fringer, O. B. (2015). The formation and fate of internal waves in the South China Sea. *Nature, 521*(7550), 65-69.

Boyce, D. G., Lewis, M. R., & Worm, B. (2010). Global phytoplankton decline over the past century. *Nature, 466*(7306), 591-596.

Carvalho, F., Kohut, J., Oliver, M. J., & Schofield, O. (2017). Defining the ecologically relevant mixed-layer depth for Antarctica's coastal seas. *Geophysical Research Letters, 44*(1), 338-345.

Chavez, F. P., Messie, M., & Pennington, J. T. (2011). Marine primary production in relation to climate variability and change. *Annual Review Marine Science, 3*, 227-260.

Claustre, H., Morel, A., Babin, M., Cailliau, C., Marie, D., Marty, J.-C., Tailliez, D., & Vaulot, D. (1999). Variability in particle attenuation and chlorophyll fluorescence in the tropical Pacific: Scales, patterns, and biogeochemical implications. *Journal of Geophysical Research: Oceans, 104*(C2), 3401-3422.

Cronin, M. F., & Sprintall, J. (2009). Wind- and buoyancy-forced upper ocean. In Steele, J., Thorpe, S., & Turekian, K., (Eds.) *Elements of Physical Oceanography: A derivative of the Encyclopedia of Ocean Sciences* (pp. 237-245). London, United Kingdom: Academic Press.

Cullen, J. J. (2015). Subsurface chlorophyll maximum layers: enduring enigma or mystery solved? *Annual Review Marine Science, 7*, 207-239.

Falkowski, P. G., & Raven, J. A. (2013). *Aquatic photosynthesis*. Princeton, NJ, USA:

28
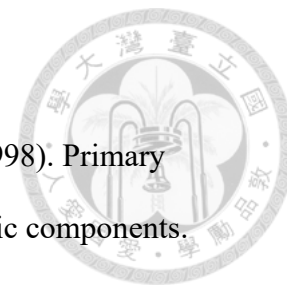
Princeton University Press.

Field, C. B., Behrenfeld, M. J., Randerson, J. T., & Falkowski, P. (1998). Primary production of the biosphere: integrating terrestrial and oceanic components. *Science, 281*(5374), 237-240.

Gardner, W. D., Chung, S. P., Richardson, M. J., & Walsh, I. D. (1995). The oceanic mixed-layer pump. *Deep Sea Research Part II: Topical Studies in Oceanography, 42*(2-3), 757-775.

Ho, T.-Y., Pan, X., Yang, H.-H., Wong, G. T. F., & Shiah, F.-K. (2015). Controls on temporal and spatial variations of phytoplankton pigment distribution in the Northern South China Sea. *Deep Sea Research Part II: Topical Studies in Oceanography, 117*, 65-85.

Kara, A. B., Rochford, P. A., & Hurlburt, H. E. (2000). An optimal definition for ocean mixed layer depth. *Journal of Geophysical Research: Oceans, 105*(C7), 16803-16821.

Karl, D. M., & Church, M. J. (2014). Microbial oceanography and the Hawaii Ocean Time-series programme. *Nature Review Microbiology, 12*(10), 699-713.

Letelier, R. M., Bidigare, R. R., Hebel, D. V., Ondrusek, M., Winn, C. D., & Karl, D. M. (1993). Temporal variability of phytoplankton community structure based on pigment analysis. *Limnology and Oceanography, 38*(7), 1420-1437.

Liu, K. K., Chao, S.-Y., Shaw, P.-T., Gong, G.-C., Chen, C.-C., & Tang, T. (2002). Monsoon-forced chlorophyll distribution and primary production in the South China Sea: observations and a numerical study. *Deep Sea Research Part I: Oceanographic Research Papers, 49*(8), 1387-1412.

Liu, K. K., Wang, L. W., Dai, M., Tseng, C. M., Yang, Y., Sui, C. H., Oey, L., Tseng, K Y., & Huang, S. M. (2013). Inter-annual variation of chlorophyll in the northern
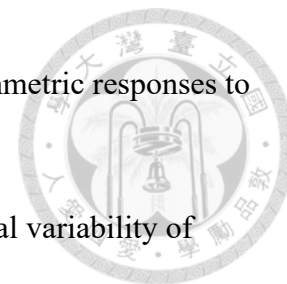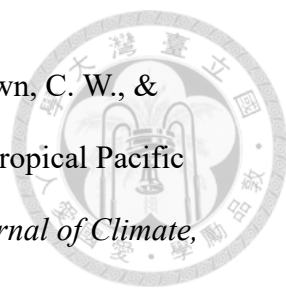
South China Sea observed at the SEATS Station and its asymmetric responses to climate oscillation. *Biogeosciences, 10*(11), 7449-7462.

Liu, M., Liu, X., Ma, A., Zhang, B., & Jin, M. (2015). Spatiotemporal variability of chlorophyll a and sea surface temperature in the northern South China Sea from 2002 to 2012. *Canadian Journal of Remote Sensing, 41*(6), 547-560.

Lyngsgaard, M. M., Markager, S., Richardson, K., Møller, E. F., & Jakobsen, H. H. (2017). How well does chlorophyll explain the seasonal variation in phytoplankton activity? *Estuaries and Coasts, 40*(5), 1263-1275.

Messié, M., & Radenac, M.-H. (2006). Seasonal variability of the surface chlorophyll in the western tropical Pacific from SeaWiFS data. *Deep Sea Research Part I: Oceanographic Research Papers, 53*(10), 1581-1600.

Mignot, A., Claustre, H., amp, apos, Ortenzio, F., Xing, X., Poteau, A., & Ras, J. (2011). From the shape of the vertical profile of in vivo fluorescence to Chlorophyll-a concentration. *Biogeosciences, 8*(8), 2391-2406.

Mignot, A., Claustre, H., Uitz, J., Poteau, A., D'Ortenzio, F., & Xing, X. (2014). Understanding the seasonal dynamics of phytoplankton biomass and the deep chlorophyll maximum in oligotrophic environments: A Bio-Argo float investigation. *Global Biogeochemical Cycles, 28*(8), 856-876.

Morel, F. M. M., & Price, N. M. (2003). The biogeochemical cycles of trace metals in the oceans. *Science, 300*(5621), 944-947.

Murray, A. P., Gibbs, C. F., Longmore, A. R., & Flett, D. J. (1986). Determination of chlorophyll in marine waters: intercomparison of a rapid HPLC method with full HPLC, spectrophotometric and fluorometric methods. *Marine Chemistry, 19*(3), 211-227.

Neveux, J. (2003). Diel dynamics of chlorophylls in high-nutrient, low-chlorophyll

waters of the equatorial Pacific (180°): Interactions of growth, grazing, physiological responses, and mixing. *Journal of Geophysical Research, 108*(C12) 5-1 - 5-17.

Pörtner, H.-O., Karl, D. M., Boyd, P. W., Cheung, W., Lluch-Cota, S. E., Nojiri, Y., Schmidt, D. N., Zavialov, P. O., Alheit J., & Aristegui, J. (2014). Ocean systems. In Field, C. B., Barros, V. R., Dokken, D.J., Mach, K. J., Mastrandrea, M. D., Bilir, T. E., Chatterjee, M., Ebi, K. L., Estrada, Y. O., Genova, R. C., Girma, B., Kissel, E. S., Levy, A. N., MacCracken, S., Mastrandrea, P. R., & White, L. L. (Eds.) *Climate change 2014: impacts, adaptation, and vulnerability. Part A: global and sectoral aspects. contribution of working group II to the fifth assessment report of the intergovernmental panel on climate change* (pp. 411-484). Cambridge, United Kingdom and New York, NY, USA: Cambridge University Press.

Pan, X., Wong, G. T. F., Tai, J.-H., & Ho, T.-Y. (2015). Climatology of physical hydrographic and biological characteristics of the Northern South China Sea Shelf-sea (NoSoCS) and adjacent waters: Observations from satellite remote sensing. *Deep Sea Research Part II: Topical Studies in Oceanography, 117*, 10-22.

Qiu, Y., Lin, Z., & Wang, Y. (2010). Responses of fish production to fishing and climate variability in the northern South China Sea. *Progress in Oceanography, 85*(3-4), 197-212.

Ryther, J. H. (1956). Photosynthesis in the Ocean as a Function of Light Intensity. *Limnology and Oceanography, 1*(1), 61-70.

Sarmiento, J. L., & Gruber, N. (2006). *Ocean biogeochemical dynamics* (pp. 150-154). Princen, NJ, USA: Princeton University Press.

Schollaert Uz, S., Busalacchi, A. J., Smith, T. M., Evans, M. N., Brown, C. W., & Hackert, E. C. (2017). Interannual and decadal variability in tropical Pacific chlorophyll from a statistical reconstruction: 1958–2008. *Journal of Climate, 30*(18), 7293-7315.

Shaw, P.-T., & Chao, S.-Y. (1994). Surface circulation in the South China sea. *Deep Sea Research Part I: Oceanographic Research Papers, 41*(11-12), 1663-1683.

Siegel, D. A., Dickey, T., Washburn, L., Hamilton, M. K., & Mitchell, B. (1989). Optical determination of particulate abundance and production variations in the oligotrophic ocean. *Deep Sea Research Part A. Oceanographic Research Papers, 36*(2), 211-222.

Strickland, J. D. H., & Parsons, T. R. (1968) *A Practical Handbook of Seawater Analysis* (pp. 185-205). Ottawa, Canada: Bulletin Fisheries Research Board of Canada.

Somavilla, R., Gonzalez-Pola, C., & Fernandez-Diaz, J. (2017). The warmer the ocean surface, the shallower the mixed layer. How much of this is true? *Journal of Geophysical Research: Oceans, 122*(9), 7698-7716.

Tai, J.-H., Wong, G. T. F., & Pan, X. (2017). Upper water structure and mixed layer depth in tropical waters: The SEATS station in the northern South China Sea. *Terrestrial, Atmospheric and Oceanic Sciences, 28*(6), 1019-1032.

Toseland, A., Daines, S. J., Clark, J. R., Kirkham, A., Strauss, J., Uhlig, C., Lenton, T. M., Valentin, K., Pearson, G. A., & Moulton, V. (2013). The impact of temperature on marine phytoplankton resource allocation and metabolism. *Nature Climate Change, 3*(11), 979-984.

Tseng, C.-M., Wong, G. T. F., Lin, I.-I, Wu, C.-R, & Liu, K.-K. (2005). A unique seasonal pattern in phytoplankton biomass in low-latitude waters in the South

China Sea. *Geophysical Research Letters, 32*(8), L08608.

Vaulot, D., & Marie, D. (1999). Diel variability of photosynthetic picoplankton in the equatorial Pacific. *Journal of Geophysical Research: Oceans, 104*(C2), 3297-3310.

Winder, M., & Cloern, J. E. (2010). The annual cycles of phytoplankton biomass. *Philosophical Transactions of the Royal Society B: Biological Sciences, 365*(1555), 3215-3226.

Winder, M., & Sommer, U. (2012). Phytoplankton response to a changing climate. *Hydrobiologia, 698*(1), 5-16.

Wong, G. T. F., Ku, T.-L., Liu, H., & Mulholland, M. (2015). The oceanography of the Northern south China Sea Shelf-Sea (NoSoCS) and its adjacent waters — overview and highlights. *Deep Sea Research Part II: Topical Studies in Oceanography, 117*, 3-9.

Wong, G. T. F., Pan, X., Li, K.-Y., Shiah, F.-K., Ho, T.-Y., & Guo, X. (2015). Hydrography and nutrient dynamics in the Northern South China Sea Shelf-sea (NoSoCS). *Deep Sea Research Part II: Topical Studies in Oceanography, 117*, 23-40.

Wood, E., & Corcoran, E. F. (1966). Diurnal variation in phytoplankton. *Bullentin of Marine Science, 16*(3), 383-403.

Woods, J., & Onken, R. (1982). Diurnal variation and primary production in the ocean preliminary results of a Lagrangian ensemble model. *Journal of Plankton Research, 4*(3), 735-756.

Zhao, H., Tang, D., & Wang, Y. (2008). Comparison of phytoplankton blooms triggered by two typhoons with different intensities and translation speeds in the South China Sea. *Marine Ecology Progress Series, 365*, 57-65.

Tables

Table 1. Abbreviations and symbols used in this study

| Symbol	Definition	Units
Chl-*a*	Chlorophyll-*a* concentration	mg m^{-3}
		ug/L
F_{Chl-a}	Chlorophyll fluorescence concentration calibrated with HPLC or fluorometer measured Chl-*a* concentrations	mg m^{-3}
$F_{Chl-a-10m}$	Chlorophyll fluorescence concentration calibrated with HPLC or fluorometer measured Chl-*a* at 10m depth	mg m^{-3}
[F_{Chl-a}]	Euphotic depth integrated chlorophyll fluorescence concentration between 5m to 100m depth	mg m^{-2}
MLD	Mixed layer depth	m
SCS	South China Sea	
SEATS	SouthEast Asian Time-series Study	
SST	Sea surface temperature	°C
$Z_{Chl-max}$	Chlorophyll maximum depth	m
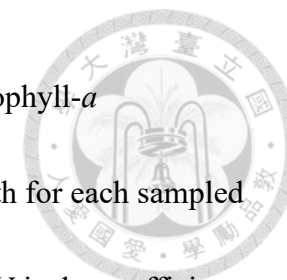
Table 2. List of cruise averaged 5-100m euphotic depth integrated chlorophyll-*a* concentrations ([F_{Chl-a}]), surface chlorophyll-*a*

concentration at 10m depth ($F_{Chl-a-10m}$), mixed layer depth (MLD), and sea surface water temperature (SST) at 10m depth for each sampled

cruise at the SEATS station from 1999 to 2019. Sample no. is the number of sampling cast taken for each cruise, and CV is the coefficient

of variance. The cruises data used for diel analysis were superscripted with a symbol ◎.

cruise	date	Month	MLD (m)	SST (℃)	[F_{Chl-a}] (mg m^{-2})	$F_{Chl-a-10m}$ (mg m^{-3})	Sample no.	[F_{Chl-a}] CV	$F_{Chl-a-10m}$ CV
OR3_561	1999/9	Sep	51	29	30	0.19	21	5%	21%
OR3_585	1999/11	Nov	51	28	18	0.09	12	8%	32%
OR3_600	2000/1	Jan	75	25	33	0.16	4	11%	8%
OR1_639	2002/3	Mar	21	27	12	0.08	30	6%	4%
OR1_664	2002/11	Nov	64	28	45	0.33	7	4%	8%
OR1_673	2003/1	Jan	84	24	23	0.27	15	13%	29%
OR1_674	2003/3	Mar	30	26	15	0.08	4	5%	4%
OR1_696	2003/10	Oct	48	29	17	0.12	9	5%	4%
OR1_705	2003/12	Dec	66	24	39	0.60	4	2%	6%
OR1_711	2004/3	Mar	58	24	30	0.16	17	11%	25%
OR1_717	2004/5	May	19	28	13	0.06	9	9%	29%
OR1_726	2004/8	Aug	34	30	18	0.08	6	6%	6%
OR1_736	2004/11/7	Nov	70	27	18	0.14	14	6%	4%
OR1_743	2005/1/22	Jan	100	23	27	0.22	10	8%	35%

35

FR1_33	2005/3/29	Mar	20	25	23	0.09	9	7%	11%
OR1_773	2005/11/9	Nov	60	28	36	0.13	11	5%	14%
OR1_780	2005/12/25	Dec	100	24	43	0.40	17	17%	28%
FR1_37	2006/7/3	Jul	42	30	22	0.12	16	11%	5%
OR1_812	2006/10/20	Oct	41	28	20	0.11	24	9%	11%
OR1_821	2007/1/15	Jan	84	24	34	0.39	31	16%	42%
◎OR1_944	2010/10/14	Oct	30	29	18	0.08	18	7%	9%
◎OR1_988	2011/12/24	Dec	78	25	27	0.43	13	24%	20%
◎OR1_1010	2012/9/1	Sep	47	29	16	0.10	11	13%	23%
◎OR1_1034	2013/4/21	Apr	33	28	16	0.07	10	6%	4%
◎OR1_1053	2013/10/16	Oct	43	28	18	0.10	7	10%	15%
◎OR1_1060	2013/12/14	Dec	74	26	22	0.19	14	9%	21%
◎OR1_1084	2014/8/5	Aug	27	29	17	0.11	14	5%	4%
◎OR1_1103	2015/4/24	Apr	24	27	22	0.08	14	15%	9%
◎OR1_1184	2017/11/15	Nov	50	28	14	0.04	16	12%	11%
◎LDG_T27	2019/1/24	Jan	64	24	19	0.25	11	7%	21%
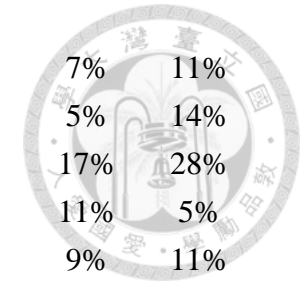
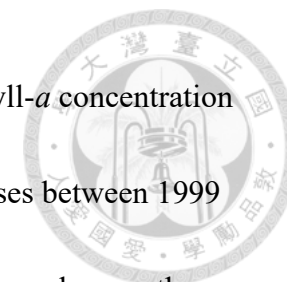Table 3. List of monthly averaged mixed layer depth (MLD), sea surface temperature (SST), depth integrated chlorophyll-*a* concentration ([F_{Chl-a}]), and surface chlorophyll-*a* concentration ($F_{Chl-a-10m}$) with standard deviation at the SEATS station from 30 cruises between 1999 and 2019. Sample no. is the number of cruises for each month, and CV is the coefficient of variance of [F_{Chl-a}] and $F_{Chl-a-10m}$ by month.

Month	MLD (m)	SST (°C)	[F_{Chl-a}] (mg m^{-2})	$F_{Chl-a-10m}$ (mg m^{-3})	Sample no.	[F_{Chl-a}] CV	$F_{Chl-a-10m}$ CV
Jan	81.47 ± 13.14	24.07 ± 0.57	27.00 ± 6.38	0.25 ± 0.09	5	24%	34%
Feb					0		
Mar	31.95 ± 17.68	25.33 ± 1.22	20.16 ± 8.14	0.10 ± 0.04	4	40%	40%
Apr	28.35 ± 6.46	27.67 ± 0.97	18.90 ± 3.76	0.08 ± 0.01	2	20%	9%
May	18.56	28.27	13.17	0.06	1		
Jun					0		
Jul	41.94	29.77	22.29	0.12	1		
Aug	30.38 ± 4.41	29.52 ± 0.47	17.60 ± 0.99	0.10 ± 0.02	2	6%	20%
Sep	49.10 ± 3.10	28.90 ± 0.52	23.23 ± 10.18	0.14 ± 0.06	2	44%	46%
Oct	40.28 ± 7.45	28.53 ± 0.54	18.35 ± 1.46	0.10 ± 0.02	3	8%	18%
Nov	58.78 ± 8.40	27.52 ± 0.32	26.08 ± 13.89	0.15 ± 0.11	5	53%	74%
Dec	79.31 ± 14.74	24.72 ± 0.74	32.74 ± 9.75	0.40 ± 0.17	4	30%	41%

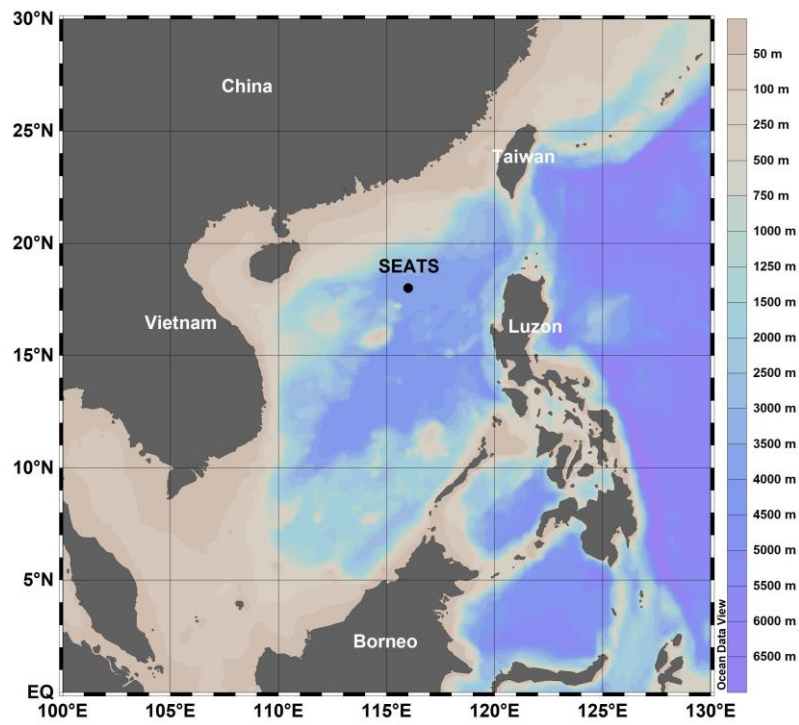**Figures**

Figure 1. Location of the SouthEast Asian Time-series Study (SEATS) station.
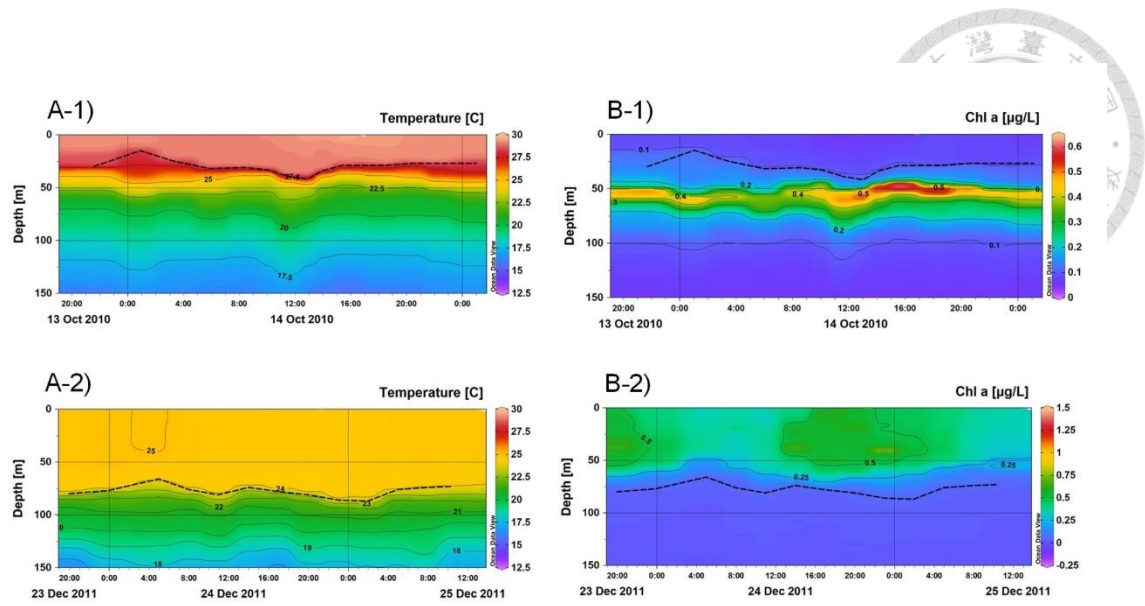
Figure 2. Diel depth contours of (A) sea water temperature and (B) chlorophyll

fluorescence concentration calibrated with Chl-*a* (F_{chl-a}) at the SEATS station for 1)

cruise OR1-944 (2010 Oct.) and 2) cruise OR1-988 (2011 Dec.) as representatives.

Black dash lines indicate the mixed layer depth.
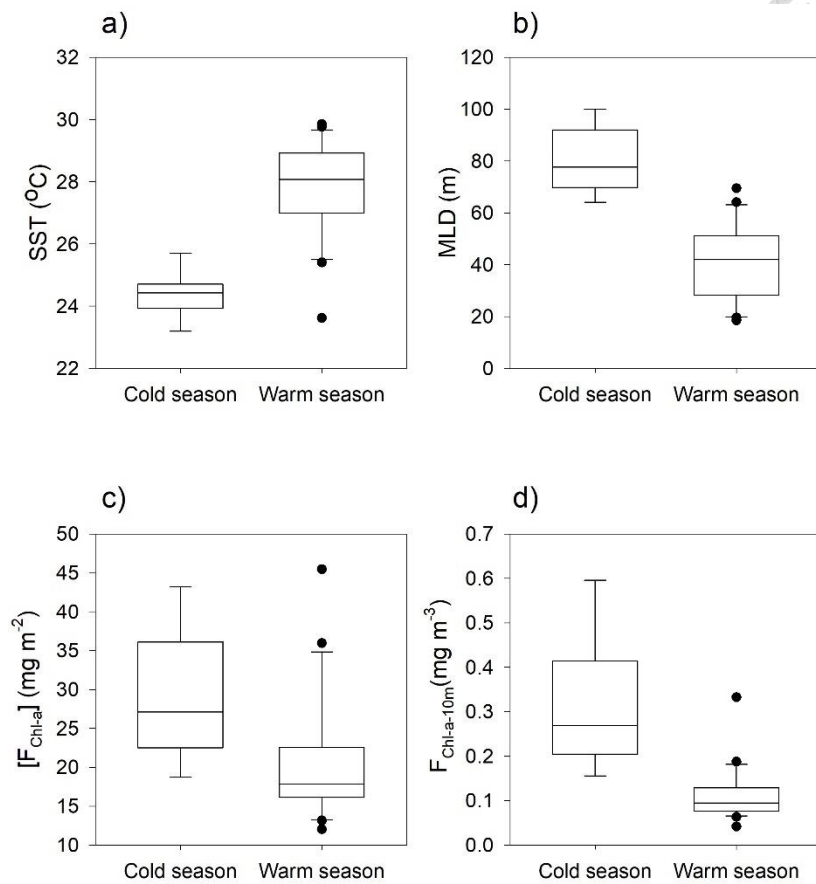
Figure 3. Box Whisker plots showing minimum (lower whisker), maximum (upper whisker), median (horizontal lines inside boxes), upper quartile (upper side of the box) and lower quartile (lower side of the box), and black dots as outliers for a) sea surface temperature (SST), b) mixed layer depth (MLD), c) depth integrated chlorophyll-*a* concentration ([F$_{Chl-a}$]), and d) surface chlorophyll-*a* concentration (F$_{Chl-a-10m}$) of cruises sampled collected during warm season (March to November), and cold season (December and January) at the SEATS station. All showed significant differences between seasons by Mann-Whitney Rank Sum Test a) *p*<0.001, b) *p*<0.001, c) *p*=0.006, and d) *p*<0.001.

40
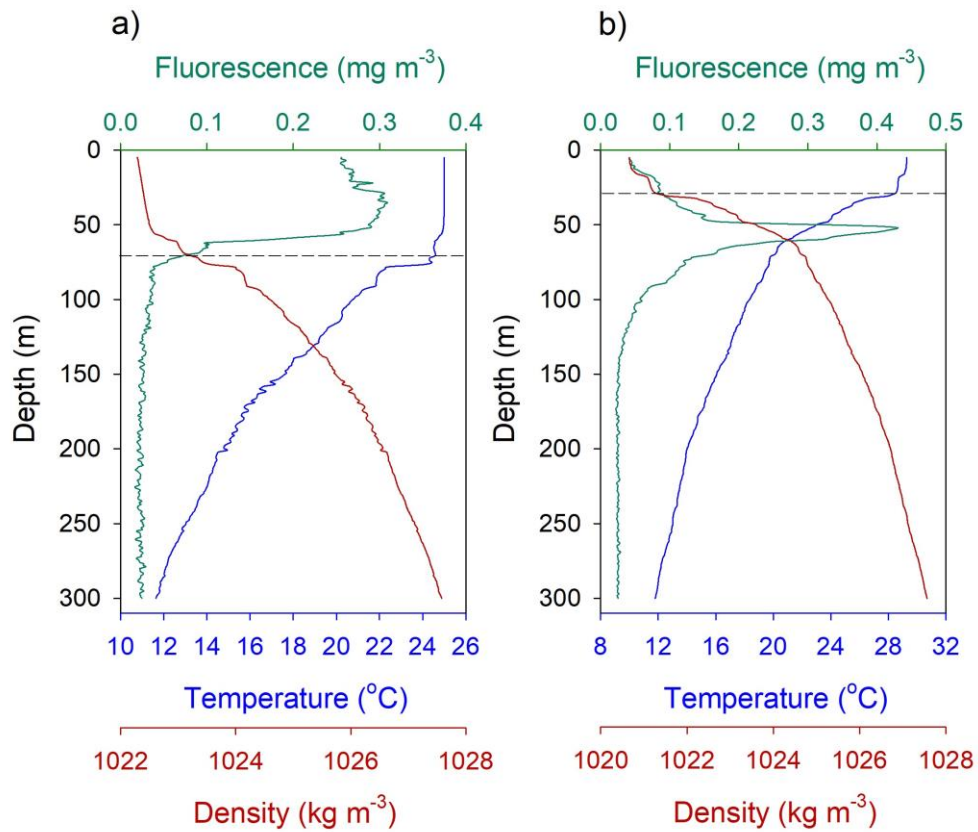
Figure 4. Typical profiles of fluorescence (green lines), temperature (blue lines) and density (red lines) of a) cold season (December and January) and b) warm season (March to November). Black dash lines indicate the mixed layer depth.
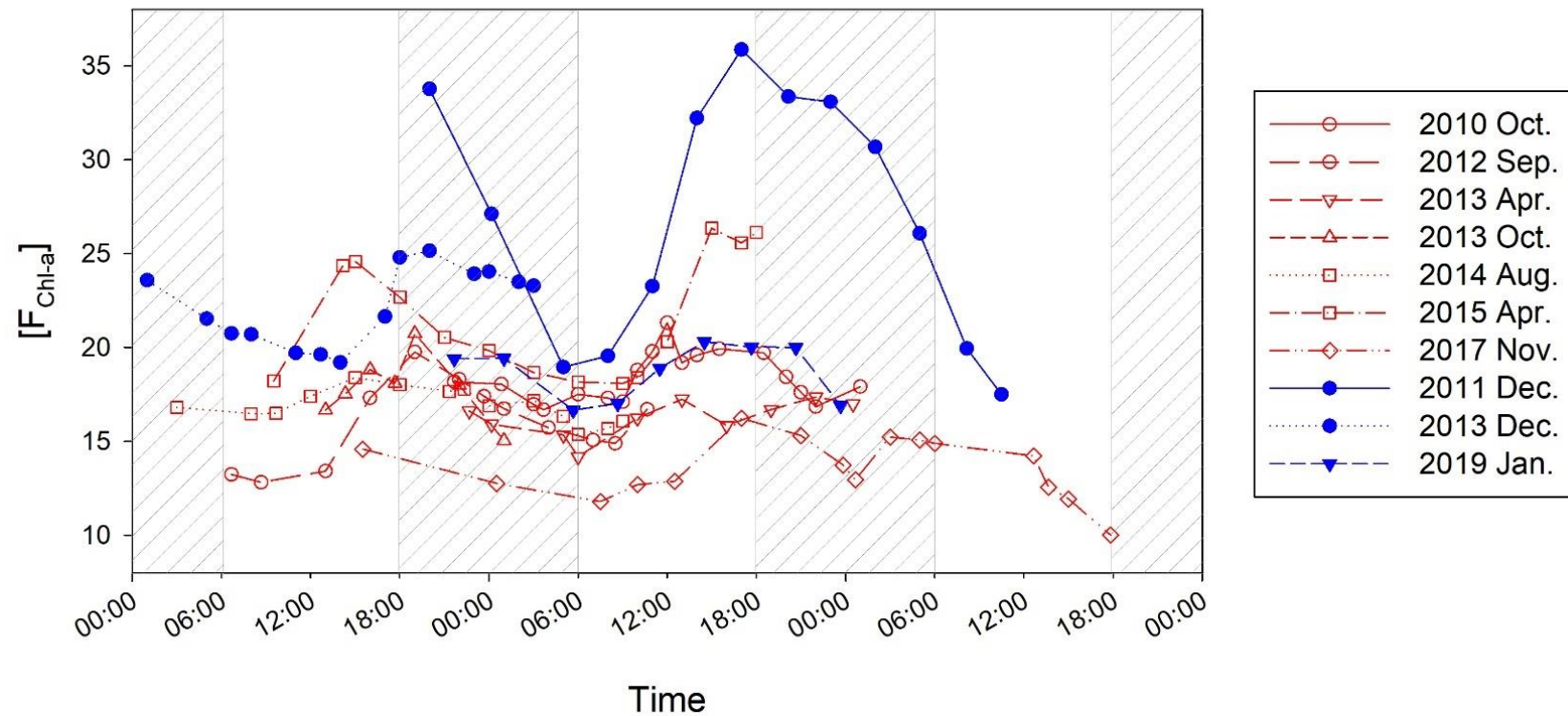
Figure 5. The diel variation of the euphotic depth integrated chlorophyll-*a* concentration ([F_{Chl-a}], mg m^{-2}) readings of the 10 cruises conducted during the period of 2010~2019 at the SEATS station. Blue symbols indicate cruises in cold season (Dec.-Jan.) and red symbols indicate cruises in warm season (Mar.-Nov.). Gray dash areas indicate night time.
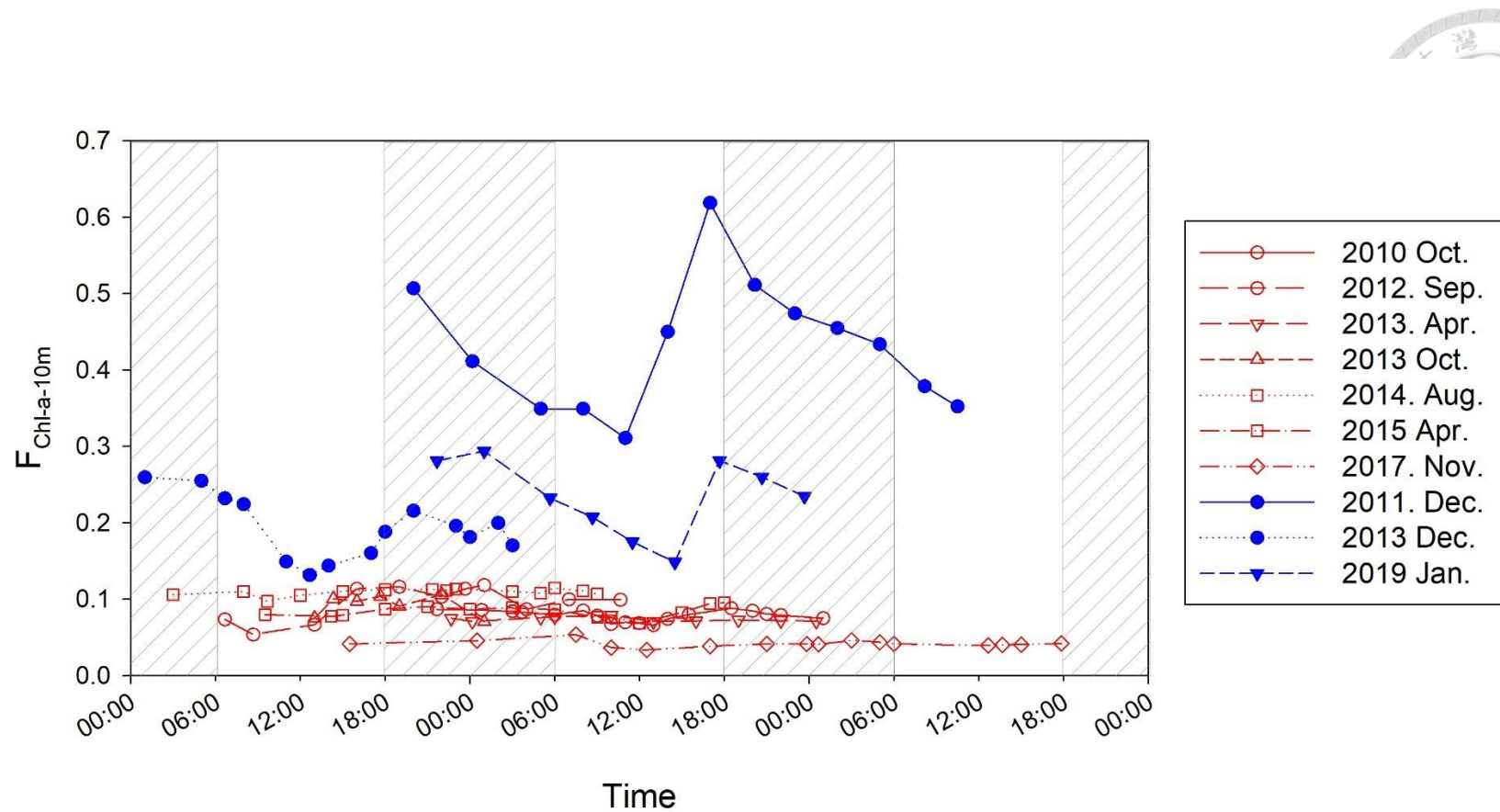
Figure 6. The diel variation of the surface chlorophyll-*a* concentration ($F_{Chl-a-10m}$, mg m^{-3}) readings of 10 cruises conducted during the period of 2010~ 2019 at the SEATS station. Blue symbols indicate cruises in cold season (Dec.-Jan.) and red symbols indicate cruises in warm season (Mar.-Nov.). Gray dash areas indicate night time.
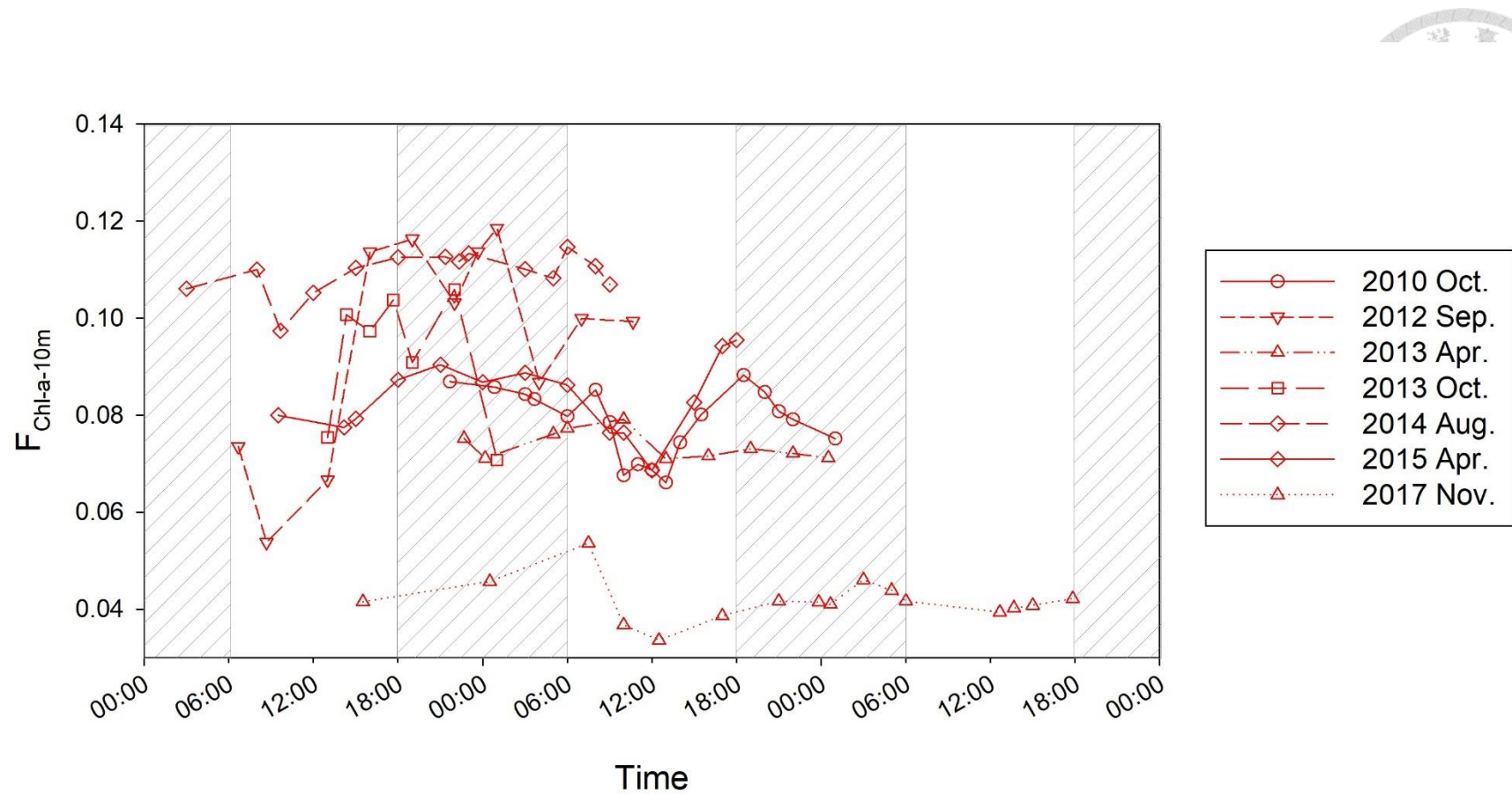
Figure 7. The diel variation of the surface chlorophyll-*a* concentration ($F_{Chl-a-10m}$, mg m^{-3}) readings of the seven warm season cruieses

conducted during the period of 2010~2019 at the SEATS station. Gray dash areas indicates night time.
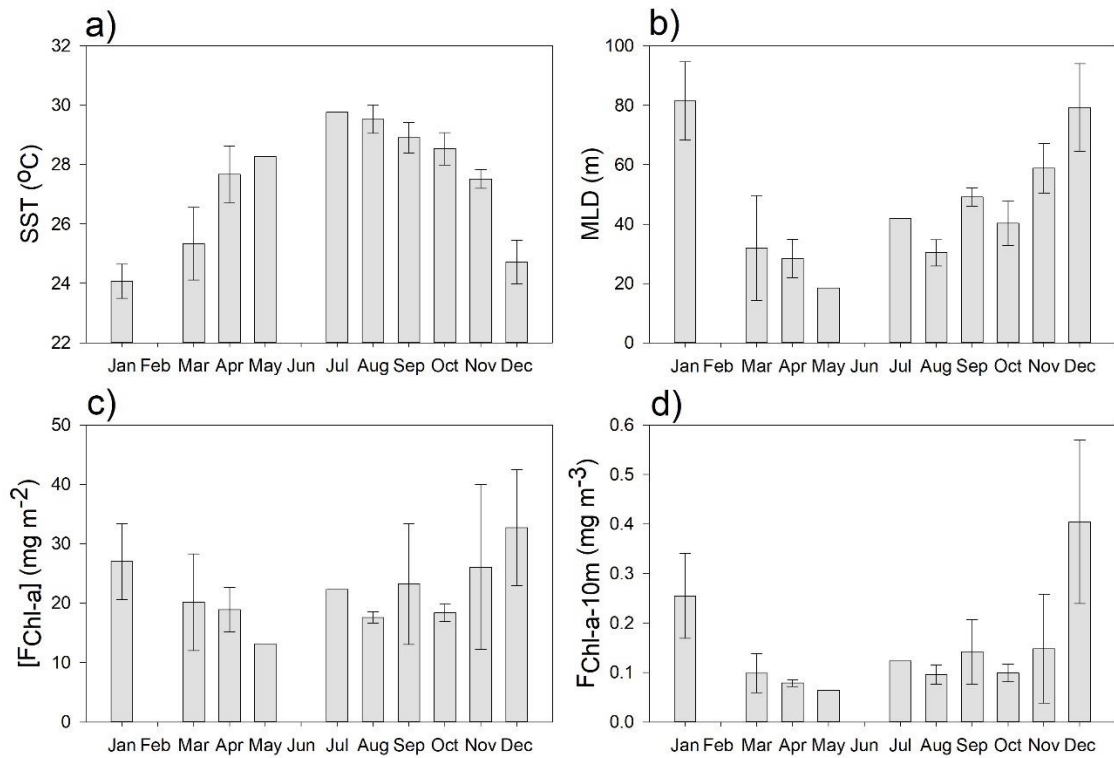
Figure 8. The monthly averaged of a) sea surface temperature (SST), b) mixed layer depth (MLD), c) euphotic depth integrated chlorophyll-*a* concentration ([F_{Chl-a}]) and d) surface chlorophyll-*a* concentration ($F_{Chl-a-10m}$) from the 30 cruises conducted during the period of 1999~2019 at the SEATS station. Error bars indicate standard deviation.
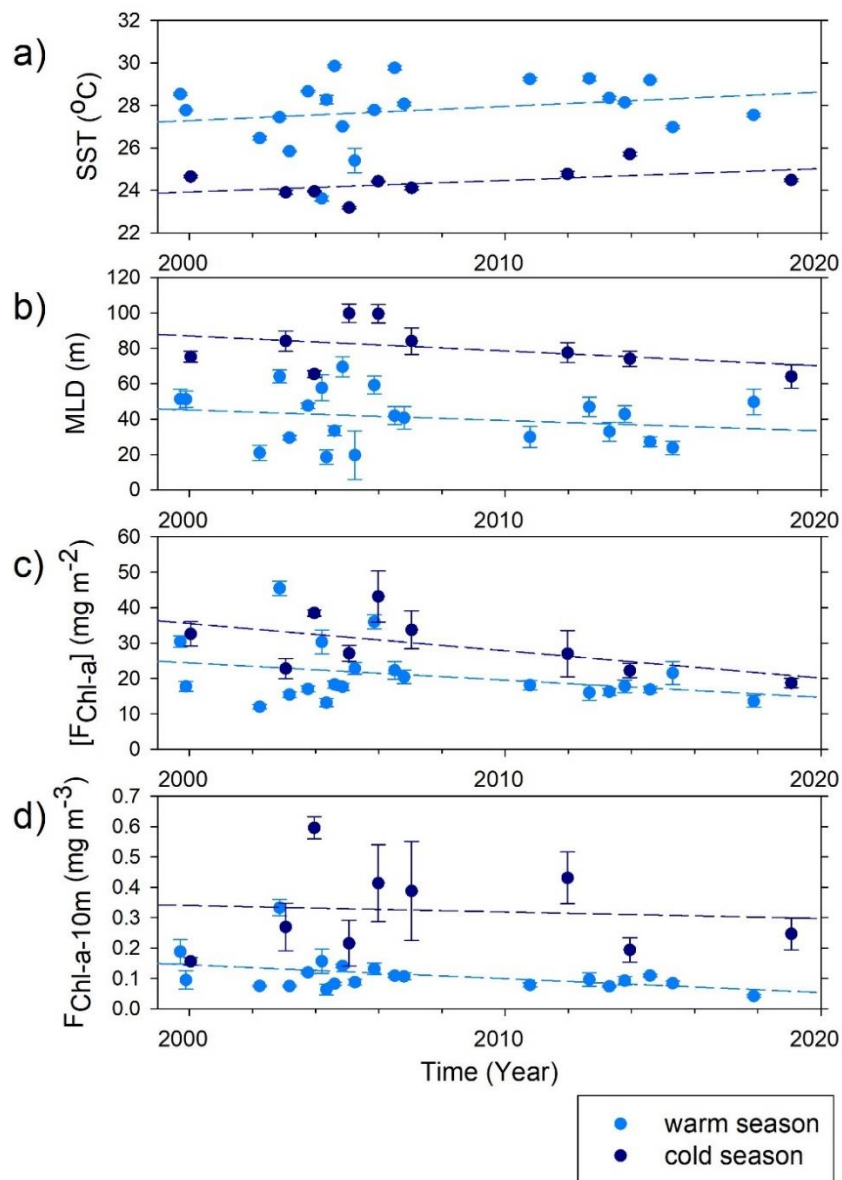
Figure 9. Decadal variations of a) sea surface temperature (SST), b) mixed layer depth (MLD), c) euphotic depth integrated chlorophyll-*a* concentration ([F_{Chl-a}]) and d) surface chlorophyll-*a* concentration ($F_{Chl-a-10m}$) from the 30 cruises conducted during the period of 1999~2019 at the SEATS station. Each dot represents the mean value of a cruise, error bars are the standard deviations, and dash lines are the best fitted lines.

Figure 10. The relationship between cruise averaged surface chlorophyll-*a*

concentration ($F_{Chl-a-10m}$) and averaged sea surface temperature (SST) for 30 cruises

from 1999 to 2019 at the SEATS station, r = -0.61, *p* < 0.0001. Error bars are standard

deviations.

Figure 11. The relationship between cruise averaged surface chlorophyll-*a* concentration ($F_{Chl-a-10m}$) and averaged mixed layer depth (MLD) for 30 cruises from 1999 to 2019 at the SEATS station, r = 0.68, *p* < 0.0001. Error bars are standard deviations.
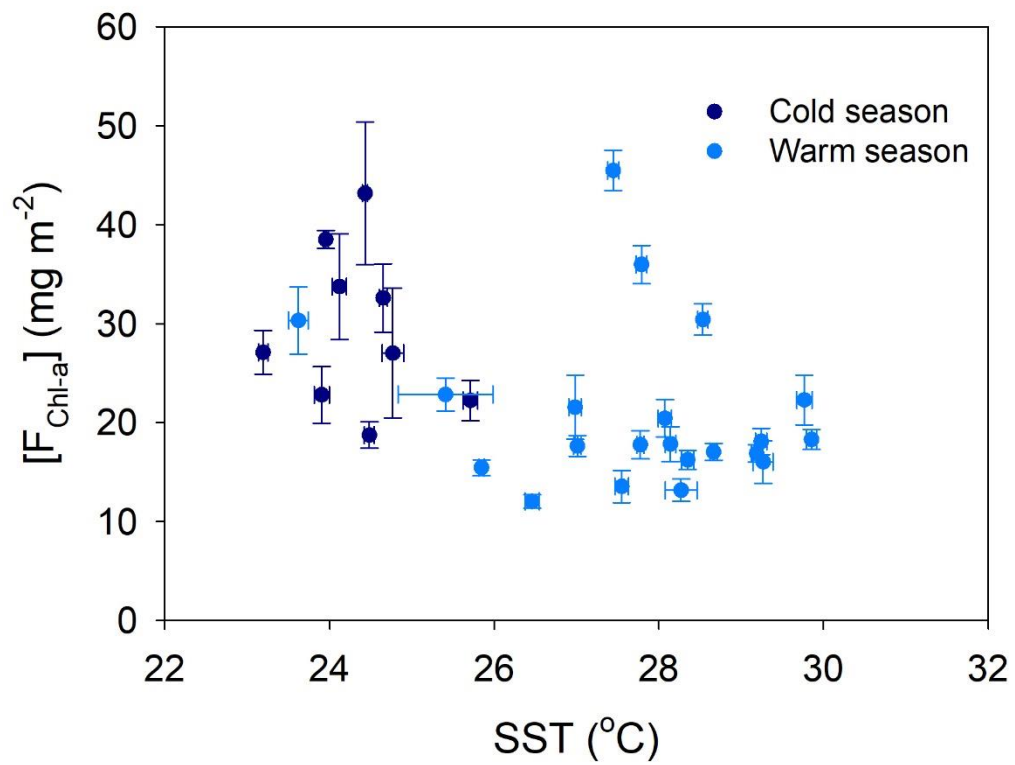
Figure 12. The relationship between cruise averaged euphotic depth integrated

chlorophyll-*a* concentration ([F_{Chl-a}]) and averaged sea surface temperature (SST) for 30

cruises from 1999 to 2019 at the SEATS station, r = -0.43, *p* = 0.012. Error bars are

standard deviations.
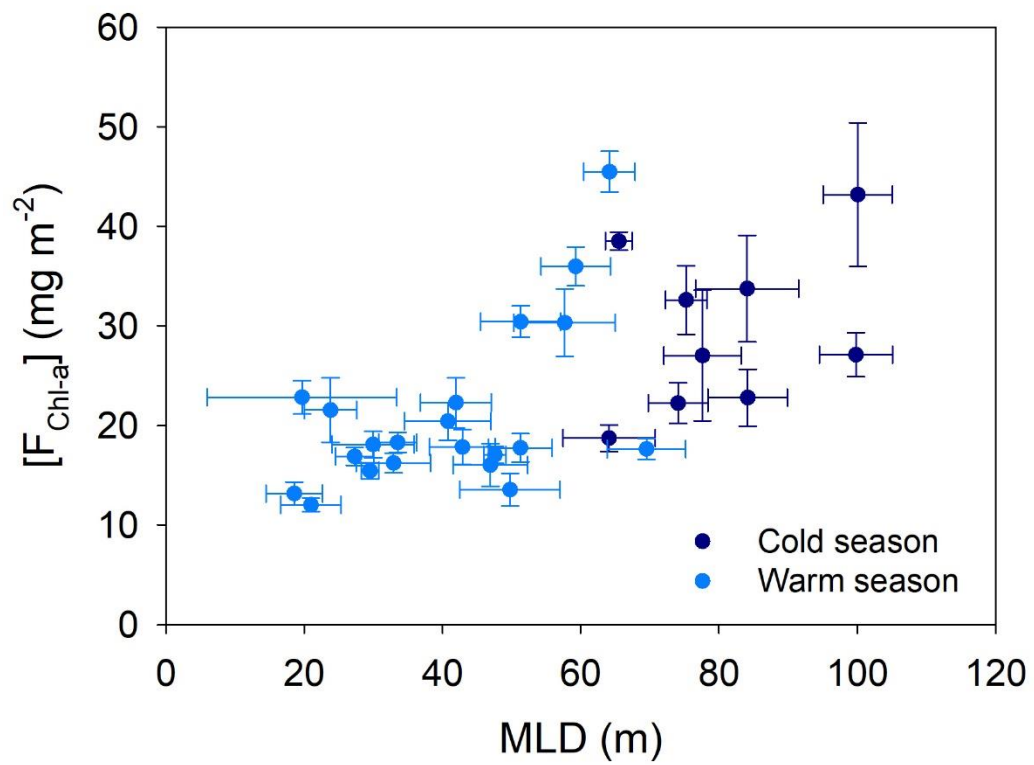
Figure 13. The relationship between cruise averaged euphotic depth integrated chlorophyll-*a* concentration ([F_{Chl-a}]) and averaged mixed layer depth (MLD) for 30 cruises from 1999 to 2019 at the SEATS station, r = 0.62, *p* < 0.0001. Error bars are standard deviations.
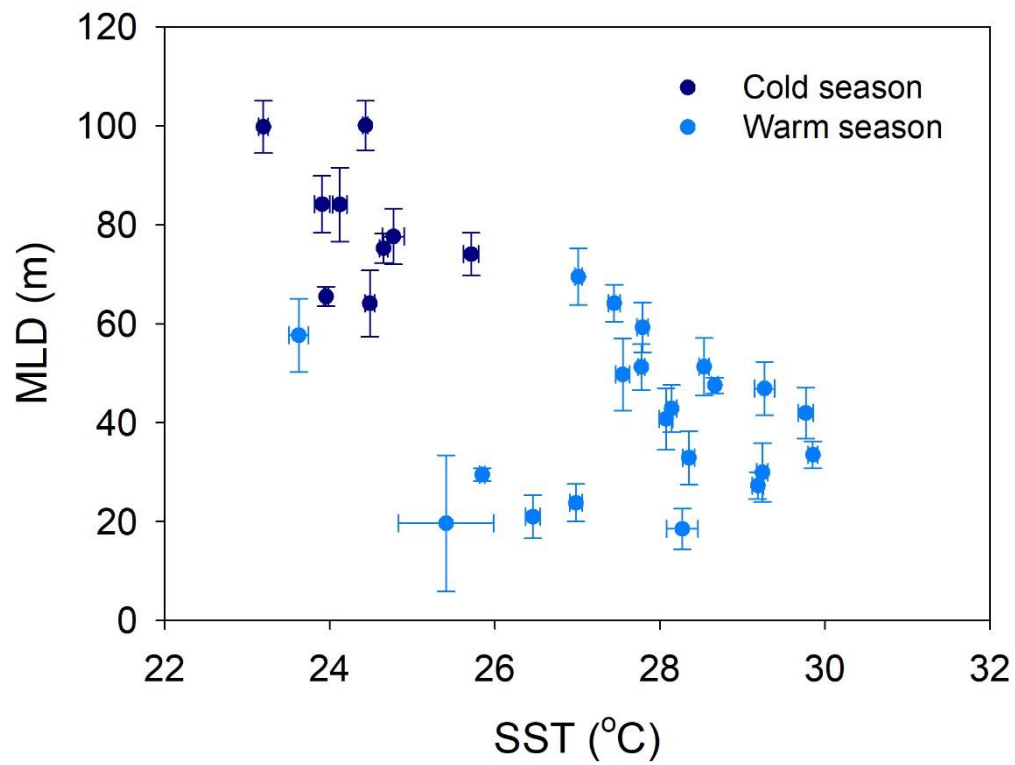
Figure 14. The relationship between cruise averaged mixed layer depth (MLD) and

averaged sea surface temperature (SST) for 30 cruises from 1999 to 2019 at the SEATS
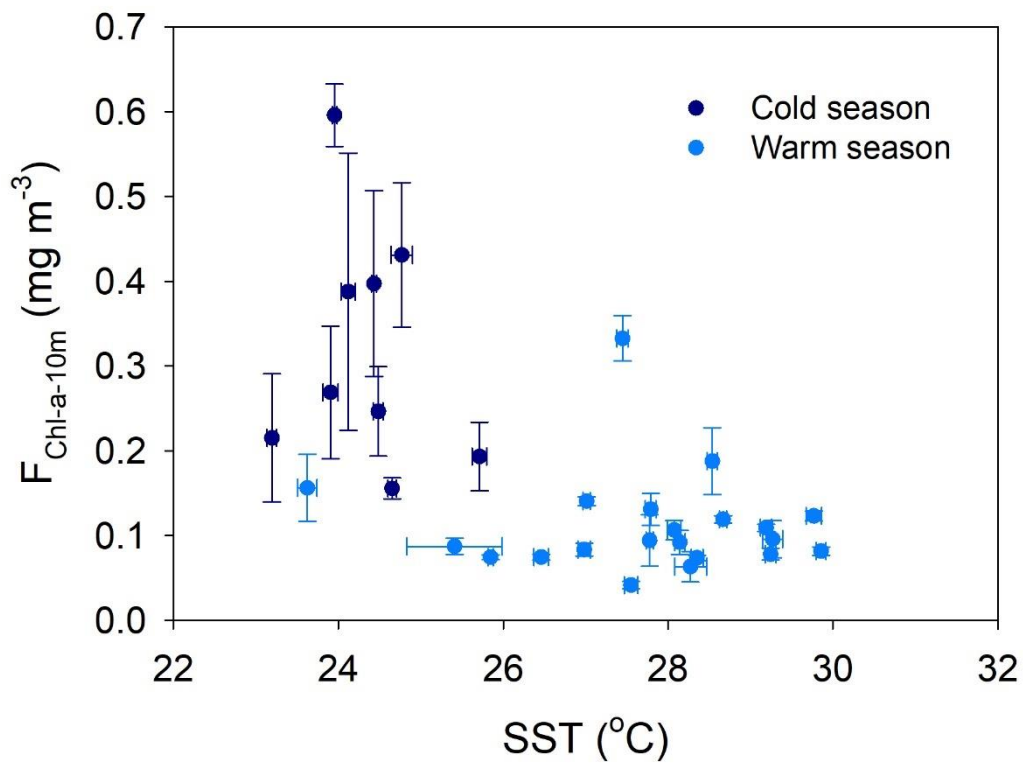
station, r = -0.65, *p* < 0.0001. Error bars are standard deviations.
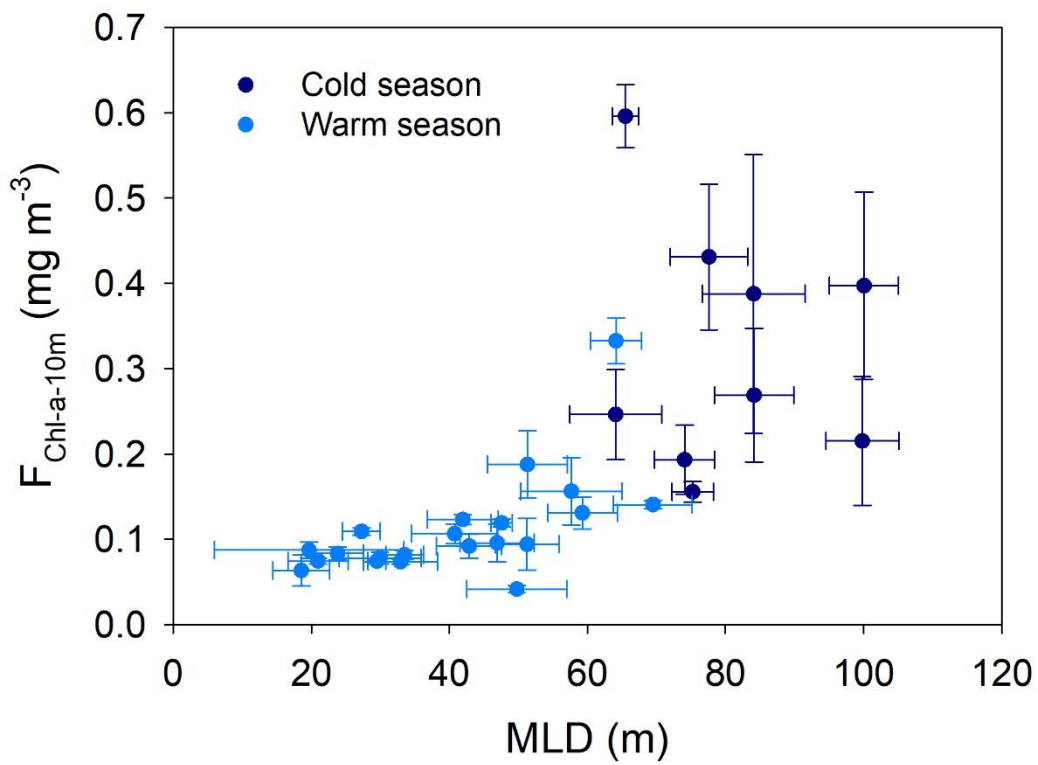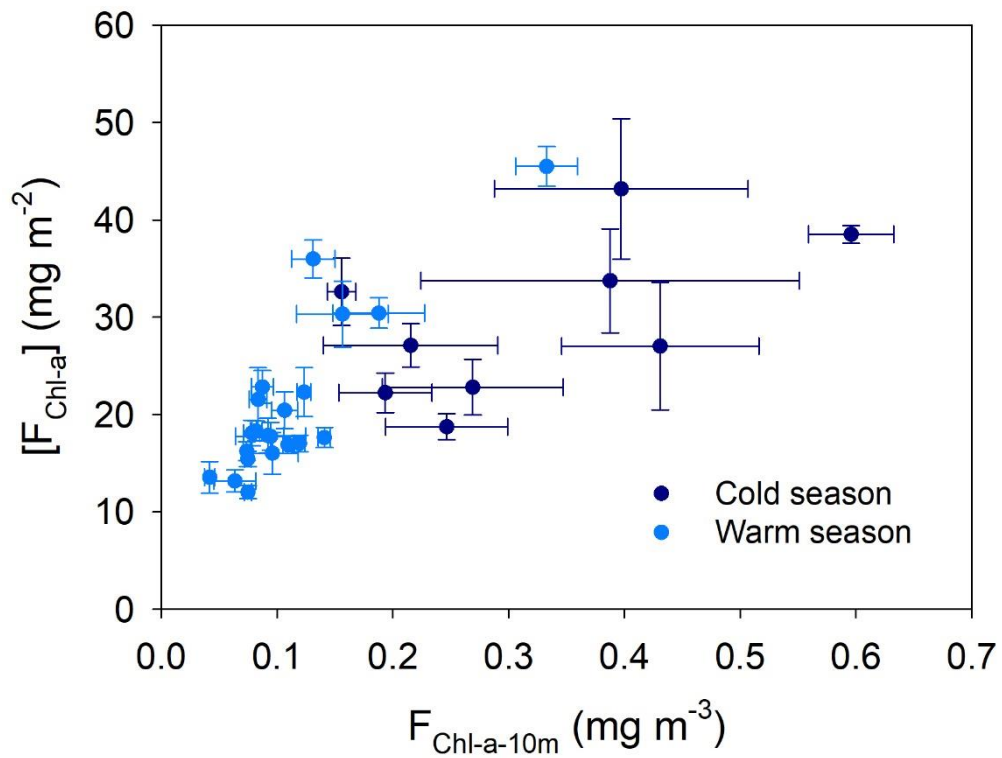
Figure 15. The relationship between cruise averaged surface chlorophyll-*a*

concentration ($F_{Chl-a-10m}$) and averaged euphotic depth integrated chlorophyll-*a*

concentration ($[F_{Chl-a}]$) for 30 cruises from 1999 to 2019 at SEATS station, r = 0.73, p <

0.0001. Error bars are standard deviations.

Appendix

Table A1. List of cruises at the SEATS station used in this study

Ship	Cruise no.	Date	Diel analysis	Chl-a analysis method
OR3	561	1999.09.19-20		Fluorometric
OR3	585	1999.11.23-26		Fluorometric
OR3	600	2000.01.16-19		Fluorometric
OR1	639	2002.03.19- 04.02		Fluorometric
OR1	664	2002.11.09-15		Fluorometric
OR1	673	2003.01.18-24		Fluorometric
OR1	674	2003.03.03-08		Fluorometric
OR1	696	2003.10.02-07		Fluorometric
OR1	705	2003.12.12-20		Fluorometric
OR1	711	2004.03.10-16		Fluorometric
OR1	717	2004.05.03-08		Fluorometric
OR1	726	2004.08.03-08		Fluorometric
OR1	736	2004.11.05-11		Fluorometric
OR1	743	2005.01.20-24		Fluorometric
FR1	33	2005.03.26-04.02		Fluorometric
OR1	773	2005.11.07-15		Fluorometric
OR1	780	2005.12.23-31		Fluorometric
FR1	37	2006.06.30-07.07		Fluorometric
OR1	812	2006.10.18-24		Fluorometric
OR1	821	2007.01.12-19		Fluorometric
OR1	944	2010.10.12-18	Yes	HPLC
OR1	988	2011.12.19-29	Yes	HPLC
OR1	1010	2012.08.28-09.04	Yes	HPLC
OR1	1034	2013.04.21-28	Yes	HPLC
OR1	1053	2013.10.14-21	Yes	HPLC
OR1	1060	2013.12.14-21	Yes	---
OR1	1084	2014.08.03-11	Yes	HPLC
OR1	1103	2015.04.20-29	Yes	HPLC
OR1	1184	2017.11.12-20	Yes	Fluorometric
LGD	T27	2019.01.24-28	Yes	Fluorometric

Table A2. Equations used for calibration of the chlorophyll fluorescence for each cruise at the SEATS station. Equations derived from the linear regression between discrete water samples with lab measured Chl-*a* and sensor (Fluorometer Aqua Track III) detected chlorophyll fluorescence.

cruise	date	Linear regression equations	
OR3_561	1999/9/19	y = 5.7406x - 0.0917	$R^2 = 0.69$
OR3_585	1999/11/23	y = 2.2403x + 0.0445	$R^2 = 0.70$
OR3_600	2000/1/17	y = 4.7598x + 0.0396	$R^2 = 0.80$
OR1_639	2002/3/25	y = 0.7705x + 0.0550	$R^2 = 0.64$
OR1_664	2002/11/11	y = 2.6651x + 0.2483	$R^2 = 0.53$
OR1_673	2003/1/20	y = 1.3033x + 0.0276	$R^2 = 0.85$
OR1_674	2003/3/5	y = 1.2622x + 0.0575	$R^2 = 0.98$
OR1_696	2003/10/4	y = 0.9889x + 0.1095	$R^2 = 0.66$
OR1_705	2003/12/16	y = 2.3819x + 0.0021	$R^2 = 0.97$
OR1_711	2004/3/12	y = 2.7095x + 0.0159	$R^2 = 0.71$
OR1_717	2004/5/5	y = 1.2427x + 0.0460	$R^2 = 0.93$
OR1_726	2004/8/6	y = 0.7713x + 0.0641	$R^2 = 0.81$
OR1_736	2004/11/7	y = 0.5990x + 0.1164	$R^2 = 0.49$
OR1_743	2005/1/22	y = 1.5218x - 0.0127	$R^2 = 0.96$
FR1_33	2005/3/29	y = 1.2043x + 0.0400	$R^2 = 0.92$
OR1_773	2005/11/9	y = 2.1315x + 0.1187	$R^2 = 0.91$
OR1_780	2005/12/25	y = 1.6155x + 0.0068	$R^2 = 0.96$
FR1_37	2006/7/3	y = 0.7797x + 0.1232	$R^2 = 0.59$
OR1_812	2006/10/20	y = 0.8377x + 0.0930	$R^2 = 0.86$
OR1_821	2007/1/15	y = 1.9269x + 0.0198	$R^2 = 0.96$
OR1_944	2010/10/14	y = 1.1131x + 0.0350	$R^2 = 0.74$

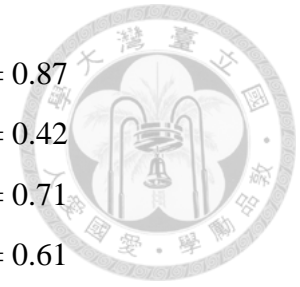|			
OR1_988	2011/12/24	y = 1.7310x - 0.0348	R² = 0.87
OR1_1010	2012/9/1	y = 0.8693x + 0.0279	R² = 0.42
OR1_1034	2013/4/21	y = 0.7702x + 0.0432	R² = 0.71
OR1_1053	2013/10/16	y = 0.8649x + 0.0381	R² = 0.61
OR1_1060	2013/12/14	y = 1.0222x + 0.0454	R² = 0.57
OR1_1084	2014/8/5	y = 0.6409x + 0.0781	R² = 0.42
OR1_1103	2015/4/24	y = 1.1992x + 0.0494	R² = 0.73
OR1_1184	2017/11/15	y = 0.4204x + 0.0053	R² = 0.70
LDG_T27	2019/1/24	y = 0.9985x - 0.0245	R² = 0.90

Table A3. Pearson's correlations between sea surface temperature (SST), mixed layer depth (MLD), euphotic depth integrated chlorophyll-a concentration ($[F_{Chl-a}]$), surface chlorophyll-a concentration ($F_{Chl-a-10m}$), and chlorophyll-a maxima depth ($Z_{Chl-max}$) for each cruise between 2010 to 2019 at the SEATS station with a diurnal sampling period, $p<0.05^*$, $p<0.01^{**}$, $p<0.001^{***}$.

1. 2010 Oct OR1 944

	SST	MLD	$[F_{Chl-a}]$	$F_{Chl-a-10m}$	$Z_{Chl-max}$
SST	1	-0.201	0.128	0.366	-0.409
MLD		1	0.445	-0.681***	0.131
$[F_{Chl-a}]$			1	-0.479*	0.066
$F_{Chl-a-10m}$				1	-0.345
$Z_{Chl-max}$					1

2. 2011 Dec OR1 988

	SST	MLD	$[F_{Chl-a}]$	$F_{Chl-a-10m}$	$Z_{Chl-max}$
SST	1	-0.561*	-0.410	-0.264	
MLD		1	0.616*	0.398	
$[F_{Chl-a}]$			1	0.887***	
$F_{Chl-a-10m}$				1	
$Z_{Chl-max}$					

3. 2012 Sep OR1 1010

	SST	MLD	$[F_{Chl-a}]$	$F_{Chl-a-10m}$	$Z_{Chl-max}$
SST	1	-0.452	-0.119	-0.147	-0.308
MLD		1	0.212	0.144	0.630*
$[F_{Chl-a}]$			1	0.880***	-0.147
$F_{Chl-a-10m}$				1	-0.336
$Z_{Chl-max}$					1

4. 2013 Apr OR1 1034

	SST	MLD	$[F_{Chl-a}]$	$F_{Chl-a-10m}$	$Z_{Chl-max}$
SST	1	0.065	0.669*	-0.315	-0.570
MLD		1	0.265	-0.583	-0.330
$[F_{Chl-a}]$			1	-0.544	-0.825***
$F_{Chl-a-10m}$				1	0.413
$Z_{Chl-max}$					1

5. 2013 Oct OR1 1053

	SST	MLD	$[F_{Chl-a}]$	$F_{Chl-a-10m}$	$Z_{Chl-max}$
SST	1	0.379	0.582	0.605	0.531
MLD		1	0.033	0.105	0.887**
$[F_{Chl-a}]$			1	0.565	0.085
$F_{Chl-a-10m}$				1	-0.077
$Z_{Chl-max}$					1

6. 2013 Dec OR1 1060

	SST	MLD	$[F_{Chl-a}]$	$F_{Chl-a-10m}$	$Z_{Chl-max}$
SST	1	-0.415	0.208	-0.659*	
MLD		1	0.387	0.623*	
$[F_{Chl-a}]$			1	0.377	
$F_{Chl-a-10m}$				1	
$Z_{Chl-max}$					

7. 2014 Aug OR1 1084

	SST	MLD	$[F_{Chl-a}]$	$F_{Chl-a-10m}$	$Z_{Chl-max}$
SST	1	-0.433	0.868***	-0.017	0.616*
MLD		1	-0.473	0.195	-0.184
$[F_{Chl-a}]$			1	0.110	0.647*
$F_{Chl-a-10m}$				1	0.316
$Z_{Chl-max}$					1
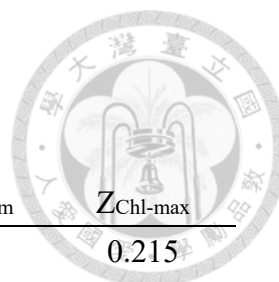
8. 2015 Apr OR1 1103

	SST	MLD	[F$_{Chl-a}$]	F$_{Chl-a-10m}$	Z$_{Chl-max}$
SST	1	-0.038	0.199	0.323	0.215
MLD		1	-0.647*	-0.259	-0.253
[F$_{Chl-a}$]			1	0.337	0.103
F$_{Chl-a-10m}$				1	0.348
Z$_{Chl-max}$					1

9. 2017 Nov OR1 1184

	SST	MLD	[F$_{Chl-a}$]	F$_{Chl-a-10m}$	Z$_{Chl-max}$
SST	1	-0.084	-0.421	-0.249	0.292
MLD		1	-0.433	-0.086	0.568*
[F$_{Chl-a}$]			1	-0.114	-0.112
F$_{Chl-a-10m}$				1	-0.316
Z$_{Chl-max}$					

10. 2019 Jan OR1 T27

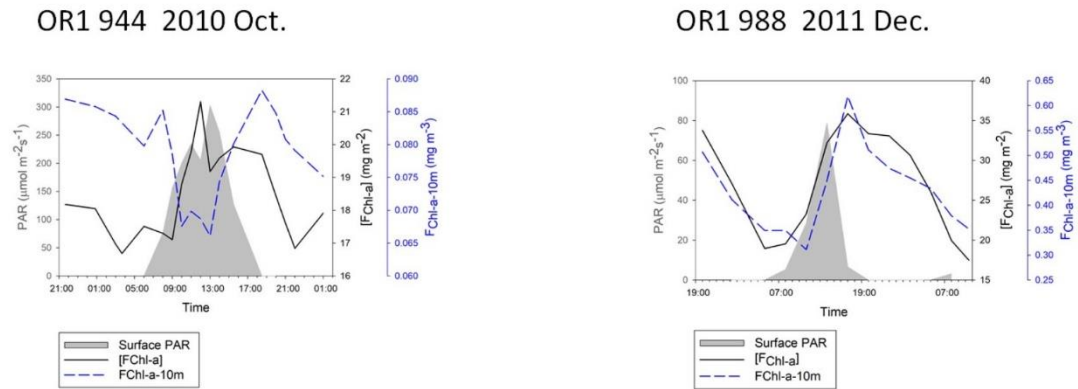|	SST	MLD	[F$_{Chl-a}$]	F$_{Chl-a-10m}$	Z$_{Chl-max}$
SST	1	-0.097	0.462	-0.024	
MLD		1	0.359	-0.631*	
[F$_{Chl-a}$]			1	0.123	
F$_{Chl-a-10m}$				1	
Z$_{Chl-max}$					

Figure A1. Diurnal variations of surface chlorophyll-*a* concentration at 10m ($F_{Chl-10m}$), euphotic depth integrated chlorophyll-*a* concentration ($[F_{Chl-a}]$), and surface photosynthetic available radiation (PAR) for cruise OR1-944 (2010 Oct.) and OR1-988 (2011 Dec.) as representatives.
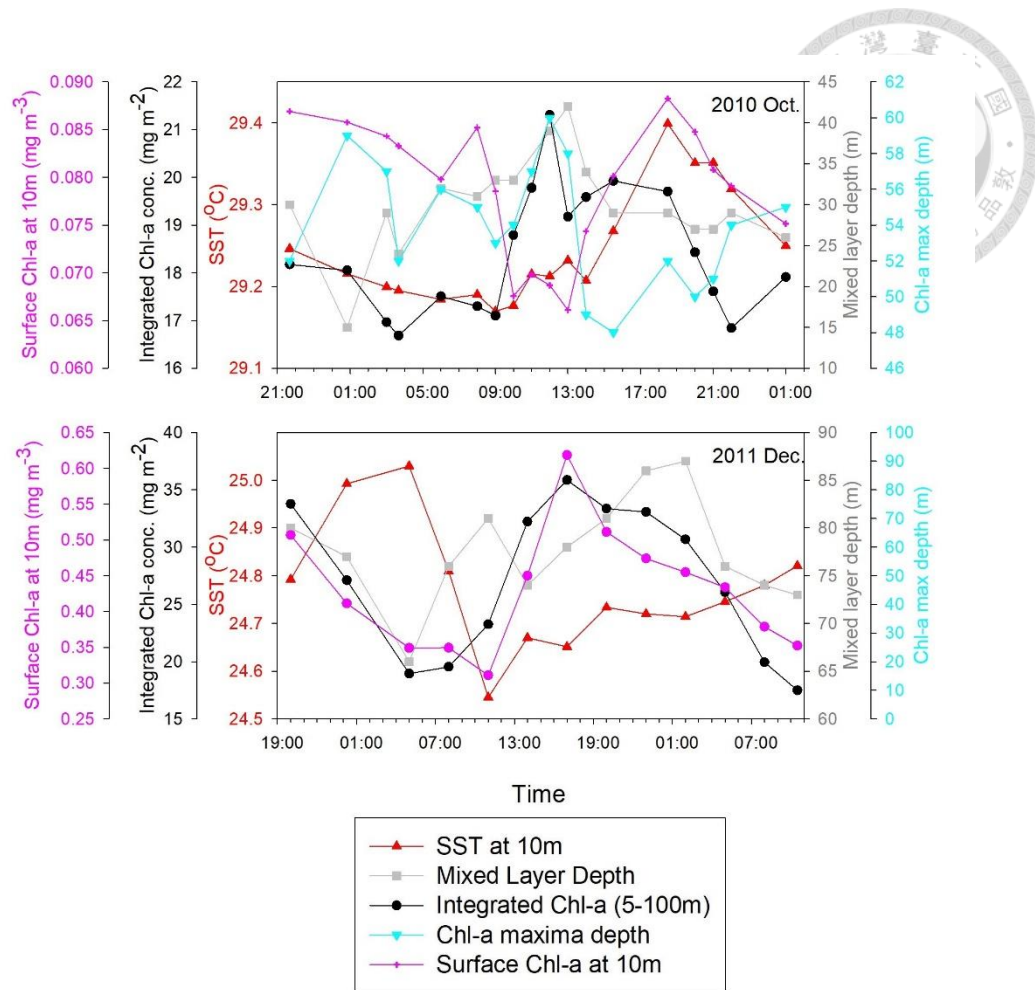
Figure A2. Diurnal variations of sea surface temperature (SST), mixed layer depth, euphotic depth integrated chlorophyll-*a* concentration, chlorophyll-*a* maxima depth, and surface chlorophyll-*a* concentration (mg m^{-3}) depth over time for cruise OR1-944 (2010 Oct.) and OR1-988 (2011 Dec.) as representatives.